学位論文

PKD1-dependent renal cystogenesis in human induced pluripotent stem cell-derived ureteric bud/collecting duct organoids

（PKD1 変異を有するヒト iPS 細胞由来尿管芽/集合管オルガノイドにおける腎嚢胞再現）

倉岡　将平

Shohei　Kuraoka

熊本大学大学院医学教育部博士課程医学専攻
小児科学

指導教員

中村　公俊　教授

熊本大学大学院医学教育部博士課程医学専攻　小児科学

西中村　隆一　教授

熊本大学大学院医学教育部博士課程医学専攻　腎臓発生学

2020年3月

学　位　論　文

論文題名　：　***PKD1*-dependent renal cystogenesis in human induced pluripotent stem cell-derived ureteric bud/collecting duct organoids**

（PKD1 変異を有するヒト iPS 細胞由来尿管芽/集合管オルガノイドにおける腎嚢胞再現）

著 者 名　：　倉岡　将平

Shohei Kuraoka

指導教員名　：　熊本大学大学院医学教育部博士課程医学専攻 小児科学　　中村　公俊　教授

熊本大学大学院医学教育部博士課程医学専攻 腎臓発生学　西中村　隆一　教授

審査委員名　：　腎臓内科学担当教授　　向山　政志

幹細胞誘導学担当教授　　江良　択実

泌尿器学担当教授　　神波　大己

機能病理学担当教授　　伊藤　隆明

2020年3月

PKD1-dependent renal cystogenesis in human induced pluripotent stem cell-derived ureteric bud/collecting duct organoids

Shohei Kuraoka[1,2], Shunsuke Tanigawa[1], Atsuhiro Taguchi[1,#], Akitsu Hotta[3], Hitoshi Nakazato[2], Kenji Osafune[4], Akio Kobayashi[1], Ryuichi Nishinakamura[1]

[1]Department of Kidney Development, Institute of Molecular Embryology and Genetics, Kumamoto University, Kumamoto 860-0811, Japan

[2]Department of Pediatrics, Faculty of Life Sciences, Kumamoto University, Kumamoto 860-8556, Japan

[3]Department of Clinical Application, Center for iPS Cell Research and Application, Kyoto University, Kyoto 606-8507, Japan

[4]Department of Cell Growth and Differentiation, Center for iPS Cell Research and Application, Kyoto University, Kyoto 606-8507, Japan

[#]Present address: Department of Genome Regulation, Max Planck Institute for Molecular Genetics, Berlin 14195, Germany

***Correspondence:**
Ryuichi Nishinakamura, Department of Kidney Development, Institute of Molecular Embryology and Genetics, Kumamoto University, 2-2-1 Honjo, Chuo-ku, Kumamoto 860-0811, Japan.

Tel.: +81-96-373-6615; Fax: +81-96-373-6618

E-mail: ryuichi@kumamoto-u.ac.jp

Running title: ADPKD cysts in ureteric bud organoids

ABSTRACT

Background Autosomal dominant polycystic kidney disease (ADPKD) is the most common hereditary kidney disease leading to renal failure, wherein multiple cysts are formed in renal tubules and collecting ducts derived from distinct precursors: the nephron progenitor and ureteric bud (UB), respectively. Recent progress in induced pluripotent stem cell (iPSC) biology has enabled cyst formation in nephron progenitor-derived human kidney organoids lacking *PKD1* and *PKD2*, the major causative genes for ADPKD. However, cyst formation in UB organoids has not been achieved, despite the prevalence of collecting duct cysts in ADPKD patients.

Methods We deleted *PKD1* in human iPSCs using CRISPR-Cas9 technology and differentially induced the cells toward nephron or UB organoids. We then investigated cyst formation in both types of kidney organoid. We also examined cyst formation in UB organoids generated from ADPKD patient-derived iPSCs.

Results As observed in nephron organoids, cysts were formed in UB organoids with homozygous *PKD1* mutations upon cAMP stimulation, and to a lesser extent, in heterozygous mutant organoids. Furthermore, UB organoids generated from ADPKD patient-derived iPSCs with a heterozygous missense mutation showed cystogenesis upon cAMP stimulation.

Conclusions We demonstrated cyst formation in *PKD1* mutant UB organoids, as well as those derived from an ADPKD patient. Our findings will serve as a valuable basis for elucidating the mechanisms of ADPKD.

Introduction

Autosomal dominant polycystic kidney disease (ADPKD) is the most common hereditary kidney disease, affecting approximately one in 1000 individuals[1]. The main features of ADPKD are multiple renal cysts that eventually cause renal failure, often accompanied by liver cysts, pancreatic cysts, and cerebral aneurysms. *PKD1* and *PKD2* are the main causative genes for ADPKD, the former accounting for approximately 85% of cases[2]. *PKD1* and *PKD2* encode polycystin-1 (PC1) and polycystin-2 (PC2) proteins, respectively. PC1 and PC2 are considered to function as a mechanosensor[3–6] and a calcium (Ca) channel[7–9], respectively. PC1 and PC2 are detected in the primary cilia of renal epithelial cells[10,11], and possibly form a complex that converts the physical force of urinary flow to Ca influx[9]. However, the function of the polycystin complex remains controversial[12].

The clinical progression of ADPKD is gradual, and most patients manifest symptoms in adulthood. The majority of ADPKD patients are heterozygous for *PKD1* mutations, initially retaining one copy of the intact allele. It is proposed that this intact allele is lost or mutated during many years of clinical progression, which may explain the late appearance of the disease (two-hit hypothesis)[13]. In contrast, other studies have shown the presence of microscopic cysts in patients at or before birth, suggesting dosage effects of PC1 proteins (haploinsufficiency) rather than loss of heterozygosity by the two-hit hypothesis[14–16]. Currently, the mechanism for ADPKD progression in response to a *PKD1* mutation in humans remains unclear.

Mouse models are frequently used to investigate the mechanisms of ADPKD. Conventional *Pkd1*-null homozygous mice show marked polycystic kidneys during embryogenesis as well as hydrops fetalis likely resulting from cardiac abnormalities, both of which can lead to embryonic

lethality[17,18]. In contrast, *Pkd1* heterozygous mice do not exhibit cysts at birth or renal failure during their lifetime, although microscopic renal cysts are observed at several months after birth[18,19]. Thus, there may be species-dependent differences in phenotypic manifestations.

The kidney develops through mutual interactions between nephron progenitors and ureteric buds (UBs), with the former contributing to the renal tubules and glomeruli, and the latter contributing to the collecting duct. Recent advances in stem cell biology have enabled the generation of nephron progenitor-derived kidney organoids (nephron organoids) from pluripotent stem cells including human cells[20–24]. Meanwhile, highly efficient gene editing in pluripotent stem cells using the CRISPR-Cas9 system enables disease modeling in organoids[25–27]. Nephron organoids lacking *PKD1* or *PKD2* were shown to form cysts[27–29], and stimulation by cAMP signaling after forskolin administration enhanced cystogenesis in these organoids[28,29]. However, most of the cysts in the organoids originated from proximal and/or distal nephron tubules because nephron organoids were used in this research. In contrast, large cysts in ADPKD patients tended to originate from collecting ducts rather than nephron tubules[30]. Indeed, tolvaptan, an antagonist of arginine vasopressin V2 receptor (AVPR2) expressed specifically in collecting ducts, is used for treatment of ADPKD patients[31], although this treatment alone cannot control or cure the disease. Thus, modeling of cyst formation in the UB/collecting duct in humans would be beneficial for this research field and future treatment. However, conventional nephron organoids lack the UB/collecting duct lineage[32,33].

Another issue is that iPSCs derived from heterozygous ADPKD patients failed to show more severe cyst formation than control cells[28]. Therefore, previous studies mainly utilized CRISPR-Cas9-mediated mutant iPSCs, and reproducible cyst modeling from patient-derived iPSCs is

awaited for allele-dependent mechanistic studies and drug screening.

We previously elucidated the developmental pathway from nascent mesoderm to nephron progenitors in mice, and successfully generated nephron organoids from human iPSCs[20,34,35]. More recently, we revealed the distinct developmental pathway to the UB through Wolffian duct progenitors, and established an induction protocol for human UBs[22]. Utilizing these two established protocols in the present study, we differentially induced *PKD1* mutant iPSCs toward UBs and nephron progenitors, and achieved cystogenesis in UB organoids with homozygous and heterozygous mutations, in addition to nephron organoids. In addition, we detected cyst formation in ADPKD patient-derived UB organoids with a heterozygous *PKD1* missense mutation.

METHODS

Construction of sgRNA and targeting vectors

A single-guide RNA (sgRNA) was designed to target exon 15 of the *PKD1* gene (target sequence: 5'-GCTCCTCCAACACGACCGTGCGG-3'; PAM sequence: GGG), and cloned into the pHL-H1-ccdB-mEF1a-H-A vector after removal of the ccdB cassette using an In-fusion HD Cloning Kit (Takara Bio) as described previously[26]. The sgRNA vector and a Cas9 expression vector (pHL-EF1a-SphcCas9-A) were first transfected into HEK293 cells using Lipofectamine 2000 (Thermo Fisher Scientific) to evaluate their activity. The target region was amplified using Target-fwd and Target-rev primers (Supplemental Table 1). When the resulting fragment was denatured and annealed, a band shift was observed, confirming the formation of a mismatched duplex resulting from small insertion or deletion mutations (indels)[36]. For the targeting vector, 5' and 3' homology arms (0.9 kb and 0.81 kb, respectively) of *PKD1* were amplified using genomic DNA from 201B7 iPSCs with the following primers: 5' arm-fwd and 5' arm-rev for 5' homology arm, 3' arm-fwd

and 3' arm-rev for 3' homology arm (Supplemental Table 1). After sequence verification, the 5' homology arm was cloned into the EcoRI site of the HR130PA-1 vector (Systems Biosciences) containing a ppluGFP2 variant[37] (precursor of TurboGFP), followed by red fluorescent protein (RFP) and a puromycin-resistance gene (Puro), and the 3' homology arm was cloned into the BamHI-SphI site of the HR130PA-1 vector.

Generation of human *PKD1* mutant iPSCs

The 201B7 human iPSC line was maintained on mouse embryonic fibroblasts as previously described[38]. The cells were pretreated with 10 μM Y-27632 (Wako; #257-00511) at 1 h prior to electroporation and a single-cell suspension was prepared using Dissociation Solution (Reprocell; #RCHETP002) followed by Accutase (Millipore). The sgRNA vector, Cas9 expression vector, and targeting vector (5 μg each) were electroporated into dissociated human iPSCs using a Super Electroporator NEPA21 (Nepagene) with two poring pulses (125 V, 2.5 ms) followed by five transfer pulses (20 V, 50 ms). The electroporated cells were plated onto puromycin-resistant DR4 feeders[39] and puromycin was added at 5 days after electroporation. The puromycin concentration was incrementally increased from 0.25 to 0.5 μg/ml at 0.05 μg/ml/day for 5 days. After the puromycin selection, 48 single colonies were picked up and screened by PCR with the following primers: Target-fwd and Target-rev, Left-fwd and Left-rev, Right-fwd and Right-rev (Supplemental Table 1). After the PCR screening, we obtained 11 candidate $PKD1^{+/+}$ clones, 17 candidate $PKD1^{+/-}$ clones, and 12 $PKD1^{-/-}$ clones. Subsequently, we sequenced the target regions in the $PKD1^{+/+}$ and $PKD1^{+/-}$ candidate clones to exclude clones with indels on the assumptive wild-type alleles. Finally, we obtained 7 $PKD1^{+/+}$, 6 $PKD1^{+/-}$, and 12 $PKD1^{-/-}$ clones. Two clones each for the $PKD1^{+/+}$, $PKD1^{+/-}$, and $PKD1^{-/-}$ genotypes (clones #2 and #5, #32 and #41, and #12 and #17, respectively) were adapted to a feeder-free condition[34], and used for subsequent analyses.

All six clones, together with their maternal cell line (210B7) used in this study, had almost normal karyotypes except for the long arm of chromosome 10. This long arm contained an additional small chromosomal fragment of unknown origin (46, XX, add(10)(q26)), possibly resulting from preferential selection of fast-growing cells. However, this abnormality was considered unlikely affect the cyst phenotypes, because *PKD1* is located on chromosome 16 (16p13.3). Although we confirmed in-frame insertion of the T2A-GFP cassette or RFP in the *PKD1* mutated alleles, GFP or RFP signals in iPSCs and nephron progenitors were not detectable by either microscopy or FACS analysis, resulting from unknown reasons possibly including silencing of the promoter regions.

Nephron organoid induction from *PKD1* mutant iPSCs

The established iPSC clones were induced toward nephron progenitors using a five-step protocol as described[22]. At day 13, some of the induced spheres were analyzed by flow cytometry to measure the percentages of $ITGA8^+/PDGFR^-$ nephron progenitors in the spheres. The percentages (31%–32%) were lower than those in our previous report using 201B7 iPSCs (40%–50%)[20] possibly because of the multiple passages upon gene manipulation. However, the variation in induction of nephron progenitor cells among the three genotypes was negligible. The remaining spheres were co-cultured with mouse embryonic spinal cord at the air-fluid interface to initiate nephron differentiation[40]. After 6 days of co-culture (day 19), the spheroids were removed from the spinal cord, and cultured in Transwell inserts (Costar; #3428) with KSR medium[41]. Subsequently, 25 μM forskolin (Wako; 067-02191) or 300 nM vasopressin (Sigma; V9879) was added to the medium from day 19 to day 25 (forskolin) or day 31 (vasopressin). Each treatment was repeated at least three times, and two clones per genotype were used in all experiments.

UB organoid induction from *PKD1* mutant iPSCs

The iPSC clones were induced toward UBs using a seven-step protocol as described[22]. At day 6.25, the percentages of $CXCR4^+/KIT^+$ Wolffian duct progenitors in the spheres were analyzed by flow cytometry. At day 12.5, the UB spheres were transferred to 24-well Transwell inserts (Costar; #3422), mounted in 150 μl of branching medium containing 50% Matrigel (Corning; #356230), and cultured in the presence of 500 μl of branching medium without Matrigel. Subsequently, 25 μM forskolin or 300 nM vasopressin was added to the medium from day 18.5 to day 30. Each treatment was repeated at least three times, and two clones per genotype were used in all experiments.

UB organoid induction from ADPKD patient-derived iPSCs

The establishment of ADPKD patient-derived iPSC lines (CiRA00007 and CiRA00009) was reported previously[42]. CiRA00007 was derived from Patient 4 with a missense mutation in *PKD1* (G3818R), and CiRA00009 was derived from Patient 6 with a nonsense mutation in *PKD1* (Q3895X). These clones had normal karyotypes and their *PKD1* mutations were confirmed to be identical to those in the patient fibroblasts by short tandem analysis[42]. The patient-derived lines, as well as the control line 201B7[38], were maintained in a feeder-free condition[34], and used for induction experiments. The concentrations of BMP4 in the first and second steps of the UB induction protocol were titrated to maximize the percentages of $CXCR4^+/KIT^+$ Wolffian duct progenitors. The optimized BMP4 concentrations were 3 ng/ml for the Patient 4-derived line and 0 ng/ml for 201B7. As the percentage of Wolffian progenitors in the Patient 6-derived line was <2% at any BMP4 concentration, the line was excluded from further analysis. All experiments using patient-derived iPSCs were performed in accordance with institutional guidelines and approved by the Licensing Committee of Kumamoto University. The names of the ethics

committees were the Ethics Committee for Epidemiological and General Research and the Ethics Committee for Human Genome and Gene Analysis Research at the Faculty of Life Science, Kumamoto University (approval numbers 1453 and 359, respectively). Analysis of patient-derived nephron organoids will be described elsewhere (K.O., manuscript in preparation).

Measurement of cyst areas

We evaluated the cyst areas in nephron organoids and UB organoids on bright-field images using ImageJ software[43]. When multiple cysts were observed in an organoid, the total area was calculated for that organoid.

Statistical analysis

Data are presented as mean ± standard error of the mean (SEM). Statistical analyses were performed by a *t*-test for differences between two groups. The Tukey–Kramer test was applied for differences among multiple groups. Differences with values of $P<0.05$ were considered statistically significant.

Result

Establishment of *PKD1* mutant iPSCs by genome editing

To examine the role of *PKD1* in human kidney cystogenesis, we inserted a drug-resistance gene cassette into the *PKD1* locus of human iPSCs by CRISPR-Cas9-mediated homologous recombination (Figure 1A). Among the 46 exons in the *PKD1* gene, we targeted exon 15 encoding the majority of the extracellular PKD repeat domains of PC1 protein (Supplemental Figure 1A, B). Exon 15 is the largest exon in the *PKD1* gene, and has been reported to contain numerous mutations, including frameshift mutations, in ADPKD patients (http://pkdb.mayo.edu/). Unlike

mice, however, humans possess *PKD1* pseudogenes[44,45], five of which have similar sequences to those in and around exon 15 (Supplemental Figure 1A). Therefore, we designed an sgRNA that specifically targeted *PKD1* exon 15, and not the pseudogenes. We introduced the sgRNA, together with the Cas9 expression vector and targeting vector, into human iPSCs. After puromycin selection, we screened for heterozygous ($PKD1^{+/-}$) and homozygous ($PKD1^{-/-}$) mutant clones by PCR (Figure 1B). Southern blotting confirmed that mutations were only introduced into the *PKD1* gene, and not the pseudogenes (Figure 1C, Supplemental Figure 1A). Indeed, $PKD1^{-/-}$ clones lacked full-length PC1 protein but expressed truncated proteins, as determined using an antibody against an N-terminal region of PC1 (Figure 1D). In $PKD1^{+/-}$ clones, reduced expression of full-length PC1 protein was observed compared with $PKD1^{+/+}$ clones (Figure 1D). Thus, we successfully generated heterozygous and homozygous *PKD1* mutant iPSC clones with intact *PKD1* pseudogenes in humans.

PKD1 mutant nephron organoids exhibit cystogenesis upon forskolin treatment

We induced the established *PKD1* mutant iPSCs toward nephron progenitors and subsequently to nephron organoids, based on our previously reported protocol[20,22] (Figure 2A). At day 13, induction of $ITGA8^+/PDGFRA^-$ nephron progenitors was comparable among the $PKD1^{+/+}$, $PKD1^{+/-}$, and $PKD1^{-/-}$ clones (Figure 2B), suggesting that the *PKD1* mutation did not affect induction of iPSCs into nephron progenitors. At day 25, all clones showed robust nephron formation: glomeruli ($WT1^+$) with proximal (LTL^+) and distal ($CDH1^+$) tubules were observed in all organoids of the three genotypes (two clones per genotype) (Figure 2C, D). However, no cysts were detected, even in $PKD1^{-/-}$ organoids, consistent with previous reports on mouse and human iPSC-derived organoids[29,46].

Because stimulation of cAMP signaling was reported to be required for renal cyst formation

in nephron organoids *in vitro*[46], we administered forskolin, an activator of cAMP signaling, to the nephron organoids at day 19 (Figure 3A). Although forskolin treatment caused cyst formation in all three genotypes, cystogenesis was most prominently observed in *PKD1*$^{-/-}$ organoids (Figure 3B). Indeed, cyst area calculations revealed significantly more severe, although variable, cystogenesis in *PKD1*$^{-/-}$ organoids compared with *PKD1*$^{+/+}$ organoids, although the latter did show mild cyst formation (Figure 3C). In all organoids examined, cysts were mainly formed in LTL^{+} proximal tubules and WT1^{+} glomerular parietal epithelial cells (Bowman capsule epithelia), irrespective of the genotypes, while cyst formation in CDH1^{+} distal tubules was less frequent (Figure 3D, Supplemental Figure 2). These observations are consistent with the early-stage phenotype of ADPKD model mice, in which cystogenesis progresses from proximal to distal tubules[47]. Primary cilia were detected on the luminal side of all cysts derived from proximal tubules regardless of the *PKD1* mutation (Supplemental Figure 3A). Their length and morphology did not appear to differ markedly among the genotypes, but the section staining precluded precise evaluation. Taken together, cyst formation was observed in human nephron organoids with homozygous or heterozygous *PKD1* mutations upon cAMP activation.

PKD1 **mutant UB organoids exhibit cystogenesis upon forskolin treatment**

Next, we induced UB organoids from the *PKD1* mutant iPSCs (Figure 4A) using our previously reported selective UB induction protocol[22]. When the UB organoids were examined at day 6.25 of the induction protocol, the percentages of CXCR4^{+}/KIT^{+} Wolffian duct progenitors were comparable among the *PKD1*$^{+/+}$, *PKD1*$^{+/-}$, and *PKD1*$^{-/-}$ clones (Figure 4B). The spheres were placed in a branching culture condition at day 12.5, and the first branching of the UB tips was observed by day 18.5 (Figure 4C). At this stage, the organoids of all three genotypes expressed marker genes for the ureteric epithelium: *RET* and *WNT11* (tip markers), *WNT9B* and *AQP2* (stalk

markers), and *GATA3* and *CALB1* (general ureteric epithelium markers), as determined by qPCR (Figure 4D). At day 30, when the UB stalks elongated and the tips underwent a few rounds of branching, RET was expressed at the tips, while cytokeratin 19 (KRT19) was abundantly expressed in the stalks in the organoids of all three genotypes (Figure 4C, E). These data indicate that the *PKD1* mutation did not affect UB induction and overall tip-stalk patterning, although the stalks of $PKD1^{-/-}$ UBs appeared shorter at day 30 (Supplemental Figure 4), possibly reflecting a mild impairment of cell polarity and/or convergent extension in the stalks[48]. Nevertheless, no cyst formation was observed without forskolin treatment even in $PKD1^{-/-}$ UB organoids, consistent with the results in nephron organoids.

UB organoids were subsequently treated with forskolin from day 18.5 (Figure 5A), resulting in cyst formation in $PKD1^{-/-}$ organoids (75.0%±22.3% for clone #12; 90%±12.2% for clone #17; n=20 per clone) at day 30 (Figure 5B, C, Supplemental Figure 5). Although not all epithelia contributed to cyst formation, bubble-like structures were formed in some of the UB stalk regions, reminiscent of the outpocketing phenomenon observed at the initial stages of cystogenesis *in vivo*[49]. In contrast, no cysts were formed in $PKD1^{+/+}$ organoids, unlike nephron organoids that showed mild cyst formation (see Figure 3B-D). Some $PKD1^{+/-}$ UB organoids (30.0%±18.7% for clone #32; 25.0%±15.8% for clone #41; n=20 per clone) also exhibited cyst formation, although the cyst areas and frequencies were less than those in $PKD1^{-/-}$ organoids (Figure 5C, D). Therefore, *PKD1*-dependent cystogenesis was achieved in human UB organoids upon cAMP activation. Primary cilia were present on the luminal side of the cysts, as seen in nephron organoids (Supplemental Figure 3B).

Cysts are composed of UB epithelia

We characterized the cysts in UB organoids using molecular markers. At day 24, reflecting an

initial stage of cyst formation, the cysts in *PKD1*$^{-/-}$ organoids expressed general ureteric epithelial markers, CALB1 and DBA, as seen in control organoids (Figure 6A). PAX2 is a transcription factor expressed in the ureteric and nephron lineages, while GATA3 is expressed in the UB and distal renal tubules. Our data showed that the cyst epithelia in *PKD1*$^{-/-}$ organoids, as well as normal epithelia in control organoids, expressed PAX2 and GATA3 at day 24 (Figure 6B). These markers were still detected at day 30 (Supplemental Figure 6A, B). A ureteric tip marker, RET, was undetectable in the cyst epithelia, while a ureteric stalk marker, KRT19, was detected (Figure 6C, Supplemental Figure 6C). These data indicate that cysts in *PKD1* mutant UB organoids were indeed derived from UB epithelia, most likely from those in the stalk regions. However, AQP2, which was expressed in the stalk regions of control organoids, was not detectable in the cyst epithelia of mutant organoids (Figure 6D, Supplemental Figure 6D), suggesting that AQP2-negative UB epithelia may have contributed to the cyst formation or failed to differentiate into the more mature AQP2-positive state. Alternatively, AQP2 expression may have been down-regulated in the cyst epithelia.

Vasopressin treatment induces cyst formation in UB organoids

Through administration of forskolin, we successfully induced cyst formation in both nephron and UB organoids. However, natural ligands that activate cAMP must exist *in vivo*. Therefore, we examined the expression of vasopressin receptors, because vasopressin (AVP) is known to induce cAMP in UB-derived collecting ducts and exacerbate cyst formation in ADPKD patients[50]. We found that the arginine vasopressin receptor 1A gene (*AVPR1A*) was expressed in UB organoids, but not in nephron organoids (Figure 7A). In contrast, *AVPR1B* and *AVPR2* were minimally detected in both types of organoid. These results were consistent with RNA-seq data for the human embryonic kidney *in vivo*[51] (Supplemental Figure 7), which detected *AVPR1A*, but not

AVPR1B or *AVPR2*, at 10–16 weeks of gestation. Immunostaining confirmed that AVPR1A was expressed in the stalk region of UB organoids and did not overlap with RET, a UB tip marker (Figure 7B). The *PKD1* mutation did not affect AVPR1A expression (Figure 7A, B). UB organoids were then treated with AVP from day 18.5 to day 30, resulting in cyst formation in *PKD1*$^{-/-}$ organoids (12.5%±7.2% for clone #12; 12.5%±7.2% for clone #17) but not in *PKD1*$^{+/-}$ or wild-type organoids (Figure 7C, D). In contrast, no cysts were formed in nephron organoids, irrespective of the genotypes, upon AVP treatment for the same duration (day 19 to day 31) (Figure 7C, D). Therefore, AVPR1A expressed in *PKD1*$^{-/-}$ UB organoids may be functional and the mutant organoids responded to AVP, its hormone ligand, to form cysts, although its efficiency for cystogenesis was not comparable to that of forskolin.

UB organoids generated from patient-derived iPSCs exhibit cystogenesis upon forskolin treatment

Finally, we applied our induction protocol for UB organoids to ADPKD patient-derived iPSCs. The patient had a heterozygous missense mutation (*PKD1* c.11452G>C; p.Gly3818Arg) and suffered numerous renal cysts, as well as hypertension, intracranial aneurysms, and subarachnoid hemorrhage[42]. In the patient's pedigree, family members with the polycystic kidney phenotype, but not those without the phenotype, had the same point mutation, suggesting that it is likely to be a disease-causing mutation. Identical missense mutations or nonsense mutations at the same position have been reported in other ADPKD families[52,53], supporting the pathogenicity of this particular mutation in our patient. By optimizing the condition in the first step of the UB induction protocol, we successfully induced CXCR4^{+}/KIT^{+} Wolffian duct progenitors from the patient-derived iPSCs, although the induction efficiency was lower than that for wild-type iPSCs (201B7) (Figure 8A). The UB organoids were moved to a branching culture condition at day 12.5 and

treated with forskolin from day 18.5 as described above (see Figure 5A). UB organoids from the patient-derived iPSCs exhibited cyst formation (15.62%±5.41%; n=4), whereas no cysts were formed in wild-type UB organoids (Figure 8B, C). The poorer tip-stalk patterns in the patient-derived organoids may result from the lower percentages of Wolffian duct progenitors compared with control organoids. The formed cyst epithelia were $PAX2^{+}/GATA3^{+}$ and $RET^{-}/KRT19^{+}$ (Figure 8D, E), consistent with the results for CRISPR-Cas9-mediated *PKD1* mutant iPSCs (see Figures 6 and 7). Therefore, we have demonstrated cyst formation from patient-derived iPSCs with a heterozygous mutation in the *PKD1* gene, although it is formally necessary to examine clones from multiple patients and to confirm cyst disappearance upon gene correction on the same genetic background (isogenic controls). Taken together with the results shown in Figure 5C, the cystogenesis caused by *PKD1* heterozygosity was not limited to the deletions generated by CRISPR-Cas9 technology, but is likely applicable to the *PKD1* mutation in the patient.

Discussion

By applying the two different induction protocols to human iPSCs lacking *PKD1*, we have demonstrated that both nephron and UB organoids exhibited cyst formation upon forskolin treatment. To the best of our knowledge, this is the first report to show cystogenesis in UB organoids. The UB organoids, but not nephron organoids, responded to vasopressin to form cysts. Furthermore, we reproducibly showed cyst formation from not only heterozygous iPSCs with an artificially truncated *PKD1* allele, but also patient-derived heterozygous *PKD1* mutant iPSCs. Thus, our UB organoids will serve as useful platforms for modeling of human ADPKD.

While nephron organoids and UB organoids both exhibited cystogenesis, their responsiveness to forskolin was different. In nephron organoids, even wild-type organoids showed cyst formation, although the severity was much less than that in *PKD1* mutant organoids.

In contrast, wild-type UB organoids never showed cyst formation, and thus abnormalities were specifically observed in *PKD1* mutant organoids. This feature may be related to differences in the nature of the epithelia: UBs were composed of epithelia that were already $CDH1^+$ at day 12.5 in our culture system, while proximal renal tubule epithelia were gradually generated and became $CDH6^+$ between days 13 and 19 through mesenchymal conversion of nephron progenitors. Thus, proximal tubules may retain the more nascent characteristics of epithelia. Alternatively, cellular adhesiveness or stiffness of $CDH1^-/CDH6^+$ proximal tubule epithelia may be weaker than that of $CDH1^+$ UB epithelia. While further studies are needed to clarify the differences in epithelial characteristics, cystogenesis specific to *PKD1* mutations with no background in wild-type organoids will make the UB organoid system more useful for drug screening to prevent cystogenesis. Because we also demonstrated cyst formation from patient-derived iPSCs, our system will be applicable to various *PKD1* alleles observed in patients.

Our data showed that cAMP signaling is required for *in vitro* cystogenesis in both nephron organoids and UB organoids, consistent with previous reports[29]. In an *ex vivo* culture setting, even *Pkd1* mutant mouse embryonic kidneys showed no cyst formation without cAMP stimulation, whereas large cysts were formed *in vivo*[46]. Although cAMP stimulation may not precisely mimic the cyst-forming signals *in vivo*, cyst formation is considered to be regulated by the balance between cAMP- and PC1/PC2-mediated signals: cAMP signaling enhances cyst formation, while Ca signaling mediated by PC1/PC2 channels antagonizes cystogenesis, probably by reducing cAMP levels[54]. Sufficient cAMP signal stimulation may not occur *in vitro*, possibly through a lack of cAMP-stimulating factors or hormones that would be present *in vivo*[55]. One such candidate is vasopressin, which works on its receptors (AVPRs) on the collecting duct cell membrane to increase intracellular cAMP levels[55]. Indeed, cyst formation in ADPKD patients is ameliorated by AVPR2 (V2) antagonists, including tolvaptan. Thus, responsiveness to vasopressin is essential for

ADPKD modeling and drug screening. Our UB organoids expressed *AVPR1A*, but not *AVPR2*. These expression patterns are consistent with those in the developing human kidney *in vivo*: *AVPR1A* is expressed at 10–20 weeks of gestation, while *AVPR2* expression is initiated later[51]. Thus, our UB organoids are likely to represent the first, or at best the second, trimester. This early expression of *AVPR1A* in the kidney may be specific to humans, because it was not observed in mice (our preliminary data). Although the functions of *AVPR1A* in human UBs remain unsolved, *AVPR1A* is expressed by endothelial cells in both humans and mice[56]. In contrast to *AVPR2* that stimulates cAMP through Gs protein, a different type of G protein, Gq, is coupled to *AVPR1A*, at least in endothelial cells[57]. Such signaling differences may explain the relatively low percentage of cyst formation in UB organoids upon vasopressin treatment, and further maturation accompanying *AVPR2* expression may be required to model ADPKD more precisely. Because nephron organoids lack AVPRs, there must be ligands other than vasopressin that can stimulate cystogenesis. Recent single-cell RNA-seq analyses of mouse and human kidneys identified many receptors in the nephron, including receptors for parathyroid hormone, somatostatin, growth hormone, and prolactin[58] (ref. 58 and our unpublished results). Searches for pro-cyst factors will advance research on cystogenesis in the nephron lineage.

Some organoids heterozygous for the *PKD1* mutation showed cyst formation within a few weeks of culture, although the severity and frequency of cystogenesis were moderate. Because deletion of the remaining wild-type allele is unlikely to occur within such a short period, the cysts in heterozygotes observed in this study were likely caused by *PKD1* haploinsufficiency. Importantly, we also showed cyst formation in UB organoids generated from ADPKD patient-derived iPSCs heterozygous for a *PKD1* mutation after forskolin treatment, although isogenic controls with the corrected gene sequence are formally required for comparison. Thus, heterozygous *PKD1* mutant epithelia are likely to be primed for exogenous signals toward

cystogenesis, which may underlie the cyst formation in ADPKD patients. However, our data do not contradict the two-hit hypothesis[13], because ADPKD patients require a long period (usually many decades) before apparent phenotypic manifestation. Deletion of the remaining wild-type allele (second hit) may occur during this long incubation period with eventual formation of numerous cysts, which cannot be reproduced in the current organoid model. It is also noteworthy that not all UBs or nephrons exhibited cyst formation even in the homozygous mutant organoids, which may be equivalent to the two-hit state. However, these observations alone cannot deny the two-hit hypothesis, because our kidney organoids represent the embryonic stage of development and immaturity of the organoids may cause different degrees of responsiveness to forskolin.

Thus, there remains much room for improvement of our UB organoids. As described above, the present organoids were immature and did not express AVPR2, although they responded to AVP, possibly through AVPR1A. Exogenous forskolin addition was required for cyst formation from *PKD1* mutant organoids. The cysts were not sufficiently large, compared with those in patients or in animal models *in vivo*. Therefore, combination of human kidney organoids with genetically engineered animal models[18,59,60] will be necessary to determine the definitive principles underlying this disease. One of the major environmental differences between our organoids and animal models is the absence and presence of urinary flow. Because organ-on-a-chip models have been developed to confer flow onto organoids[61], application of *PKD1* mutant organoids to these microdevices will be one possible option to reproduce more physiological cyst formation.

Taken together, we have demonstrated *PKD1*-dependent cystogenesis in nephron organoids and UB organoids, with responsiveness to vasopressin in the latter. We further showed cyst formation from patient-derived organoids with a heterozygous *PKD1* missense mutation. Our findings, as well as our differential induction protocols and *PKD1* mutant iPSCs, will serve as

valuable bases for modeling of ADPKD to elucidate the mechanisms underlying the disease and to screen for therapeutic chemicals.

Author Contributions

S.K. and R.N. designed experiments. S.K. performed experiments and analyses. S.T., A.T., and H.N. assisted with experiments. A.H. generated the CRISPR-Cas9 vectors. K.O. established the patient-derived iPSCs. S.K. wrote the original draft. A.K., A.T., and R.N. reviewed and edited the manuscript. A.K. and R.N. administrated the project. R.N. acquired research funding.

Acknowledgments

We thank Tomoko Ohmori and Sayoko Fujimura for technical assistance. We also thank Alison Sherwin, PhD, from Edanz Group (https://en-author-services.edanzgroup.com/) for editing a draft of this manuscript.

Financial Disclosures

K.O. is a founder and member without salary of the scientific advisory boards of iPS Portal, Inc., and a founder and chief scientific advisor of RegeNephro Co., Ltd. The other authors have nothing to disclose.

Funding

This study was partly supported by a KAKENHI grant (JP17H06177 to R.N.) from the Japan Society for the Promotion of Science and a grant (20bm0804013h0004) from the Research Center Network for Realization of Regenerative Medicine, Japan Agency for Medical Research and Development.

SUPPLEMENTAL TABLE OF CONTENTS

References

1. Yersin C, Bovet P, Wauters J, Schorderet D, Pescia G, Paccaud F: Frequency and impact of autosomal dominant polycystic kidney disease in the Seychelles (Indian Ocean). *Nephrol. Dial. Transplant.* 12: 2069–2074, 1997
2. Torres VE, Harris PC, Pirson Y: Autosomal dominant polycystic kidney disease. *Lancet* 369: 1287–1301, 2007
3. Chauvet V, Tian X, Husson H, Grimm DH, Wang T, Hieseberger T, et al.: Mechanical stimuli induce cleavage and nuclear translocation of the polycystin-1 C terminus. *J. Clin. Invest.* 114: 1433–1443, 2004
4. Nauli SM, Alenghat FJ, Luo Y, Williams E, Vassilev P, Li X, et al.: Polycystins 1 and 2 mediate mechanosensation in the primary cilium of kidney cells. *Nat. Genet.* 33: 129–137, 2003
5. Patel A, Honoré E: Polycystins and renovascular mechanosensory transduction. *Nat. Rev. Nephrol.* 6: 530–538, 2010
6. Kim S, Nie H, Nesin V, Tran U, Outeda P, Bai CX, et al.: The polycystin complex mediates Wnt/Ca2+ signalling. *Nat. Cell Biol.* 18: 752–764, 2016
7. Hanaoka K, Qian F, Boletta A, Bhunia AK, Piontek K, Tsiokas L, et al.: Co-assembly of polycystin-1 and -2 produces unique cation-permeable currents. *Nature* 408: 990–994, 2000
8. Vassilev PM, Kanazirska M, Ye C ping, Brown EM, Guo L, Chen XZ, et al.: Polycystin-2 is a novel cation channel implicated in defective intracellular Ca2+ homeostasis in polycystic kidney disease. *Biochem. Biophys. Res. Commun.* 282: 341–350, 2001
9. Su Q, Hu F, Ge X, Lei J, Yu S, Wang T, et al.: Structure of the human PKD1-PKD2 complex. *Science* 361: eaat9819, 2018

10. Foggensteiner L, Bevan AP, Thomas R, Coleman N, Boulter C, Bradley J, et al.: Cellular and subcellular distribution of polycystin-2, the protein product of the PKD2 gene. *J. Am. Soc. Nephrol.* 11: 814–827, 2000

11. Zhou J: Polycystins and Primary Cilia: Primers for Cell Cycle Progression. *Annu. Rev. Physiol.* 71: 83–113, 2009

12. Delling M, Indzhykulian AA, Liu X, Li Y, Xie T, Corey DP, et al.: Primary cilia are not calcium-responsive mechanosensors. *Nature* 531: 656–660, 2016

13. Pei Y: A 'two-hit' model of cystogenesis in autosomal dominant polycystic kidney disease? *Trends Mol. Med.* 7: 151–156, 2001

14. Boyer O, Gagnadoux M-F, Guest G, Biebuyck N, Charbit M, Salomon R, et al.: Prognosis of autosomal dominant polycystic kidney disease diagnosed in utero or at birth. *Pediatr. Nephrol.* 22: 380–388, 2007

15. Reed B, Nobakht E, Dadgar S, Bekheirnia MR, Masoumi A, Belibi F, et al.: Renal Ultrasonographic Evaluation in Children at Risk of Autosomal Dominant Polycystic Kidney Disease. *Am. J. Kidney Dis.* 56: 50–56, 2010

16. Grantham JJ, Cook LT, Wetzel LH, Cadnapaphornchai MA, Bae KT: Evidence of Extraordinary Growth in the Progressive Enlargement of Renal Cysts. *Clin. J. Am. Soc. Nephrol.* 5: 889–896, 2010

17. Lu W, Peissel B, Babakhanlou H, Pavlova A, Geng L, Fan X, et al.: Perinatal lethality with kidney and pancreas defects in mice with a targetted Pkd1 mutation. *Nat. Genet.* 17: 179–181, 1997

18. Lu W: Comparison of Pkd1-targeted mutants reveals that loss of polycystin-1 causes cystogenesis and bone defects. *Hum. Mol. Genet.* 10: 2385–2396, 2001

19. Lu W, Fan X, Basora N, Babakhanlou H, Law T, Rifai N, et al.: Late onset of renal and

hepatic cysts in Pkd1-targeted heterozygotes. *Nat. Genet.* 21: 160–161, 1999

20. Taguchi A, Kaku Y, Ohmori T, Sharmin S, Ogawa M, Sasaki H, et al.: Redefining the In Vivo Origin of Metanephric Nephron Progenitors Enables Generation of Complex Kidney Structures from Pluripotent Stem Cells. *Cell Stem Cell* 14: 53–67, 2014

21. Morizane R, Lam AQ, Freedman BS, Kishi S, Valerius MT, Bonventre J V.: Nephron organoids derived from human pluripotent stem cells model kidney development and injury. *Nat. Biotechnol.* 33: 1193–1200, 2015

22. Taguchi A, Nishinakamura R: Higher-Order Kidney Organogenesis from Pluripotent Stem Cells. *Cell Stem Cell* 21: 730-746.e6, 2017

23. Mae S-I, Ryosaka M, Toyoda T, Matsuse K, Oshima Y, et al.: Generation of branching ureteric bud tissues from human pluripotent stem cells. *Biochem. Biophys. Res. Commun.* 495: 954–961, 2018

24. Takasato M, Er PX, Chiu HS, Maier B, Baillie GJ, Ferguson C, et al.: Kidney organoids from human iPS cells contain multiple lineages and model human nephrogenesis. *Nature* 526: 564–568, 2015

25. Jinek M, Chylinski K, Fonfara I, Hauer M, Doudna JA, Charpentier E: A Programmable Dual-RNA-Guided DNA Endonuclease in Adaptive Bacterial Immunity. *Science* 337: 816–821, 2012

26. Li HL, Gee P, Ishida K, Hotta A: Efficient genomic correction methods in human iPS cells using CRISPR–Cas9 system. *Methods* 101: 27–35, 2016

27. Freedman BS, Brooks CR, Lam AQ, Fu H, Morizane R, Agrawal V, et al.: Modelling kidney disease with CRISPR-mutant kidney organoids derived from human pluripotent epiblast spheroids. *Nat. Commun.* 6: 8715, 2015

28. Cruz NM, Song X, Czerniecki SM, Gulieva RE, Churchill AJ, Kim YK, et al.: Organoid

cystogenesis reveals a critical role of microenvironment in human polycystic kidney disease. *Nat. Mater.* 16: 1112–1119, 2017

29. Czerniecki SM, Cruz NM, Harder JL, Menon R, Annis J, Otto EA, et al.: High-Throughput Screening Enhances Kidney Organoid Differentiation from Human Pluripotent Stem Cells and Enables Automated Multidimensional Phenotyping. *Cell Stem Cell* 22: 929-940.e4, 2018

30. Devuyst O, Burrow CR, Smith BL, Agre P, Knepper MA, Wilson PD: Expression of aquaporins-1 and -2 during nephrogenesis and in autosomal dominant polycystic kidney disease. *Am. J. Physiol. Physiol.* 271: F169–F183, 1996

31. Baur BP, Meaney CJ: Review of Tolvaptan for Autosomal Dominant Polycystic Kidney Disease. *Pharmacother. J. Hum. Pharmacol. Drug Ther.* 34: 605–616, 2014

32. Wu H, Uchimura K, Donnelly EL, Kirita Y, Morris SA, Humphreys BD: Comparative Analysis and Refinement of Human PSC-Derived Kidney Organoid Differentiation with Single-Cell Transcriptomics. *Cell Stem Cell* 23: 869-881.e8, 2018

33. Combes AN, Zappia L, Er PX, Oshlack A, Little MH: Single-cell analysis reveals congruence between kidney organoids and human fetal kidney. *Genome Med.* 11: 3, 2019

34. Sharmin S, Taguchi A, Kaku Y, Yoshimura Y, Ohmori T, Sakuma T, et al.: Human Induced Pluripotent Stem Cell–Derived Podocytes Mature into Vascularized Glomeruli upon Experimental Transplantation. *J. Am. Soc. Nephrol.* 27: 1778–1791, 2016

35. Yoshimura Y, Taguchi A, Tanigawa S, Yatsuda J, Kamba T, Takahashi S, et al.: Manipulation of Nephron-Patterning Signals Enables Selective Induction of Podocytes from Human Pluripotent Stem Cells. *J. Am. Soc. Nephrol.* 30: 304–321, 2019

36. Nakagawa Y, Yamamoto T, Suzuki K-I, Araki K, Takeda N, Ohmuraya M, et al.:

Screening Methods to Identify TALEN-Mediated Knockout Mice. *Exp. Anim.* 63: 79–84, 2014

37. Evdokimov AG, Pokross ME, Egorov NS, Zaraisky AG, Yampolsky I V., Merzlyak EM, et al.: Structural basis for the fast maturation of Arthropoda green fluorescent protein. *EMBO Rep.* 7: 1006–1012, 2006

38. Takahashi K, Tanabe K, Ohnuki M, Narita M, Ichisaka T, Tomoda K, et al: Induction of Pluripotent Stem Cells from Adult Human Fibroblasts by Defined Factors. *Cell* 131: 861–872, 2007

39. Tucker KL, Wang Y, Dausman J, Jaenisch R: A transgenic mouse strain expressing four drug-selectable marker genes. *Nucleic Acids Res.* 25: 3745–3746, 1997

40. Yoshimura Y, Taguchi A, Nishinakamura R: Generation of a Three-Dimensional Kidney Structure from Pluripotent Stem Cells. In: *Organ Regeneration: 3D Stem Cell Culture & Manipulation*, edited by Tsuji T, pp 179–193, 2017

41. Li Z, Araoka T, Wu J, Liao H-K, Li M, Lazo M, et al.: 3D Culture Supports Long-Term Expansion of Mouse and Human Nephrogenic Progenitors. *Cell Stem Cell* 19: 516–529, 2016

42. Ameku T, Taura D, Sone M, Numata T, Nakamura M, Shiota F, et al.: Identification of MMP1 as a novel risk factor for intracranial aneurysms in ADPKD using iPSC models. *Sci. Rep.* 6: 30013, 2016

43. Schneider CA, Rasband WS, Eliceiri KW: NIH Image to ImageJ: 25 years of image analysis. *Nat. Methods* 9: 671–675, 2012

44. Roelfsema JH, Spruit L, Saris JJ, Chang P, Pirson Y, van Ommen G-JB, et al.: Mutation Detection in the Repeated Part of the PKD1 Gene. *Am. J. Hum. Genet.* 61: 1044–1052, 1997

45. Kirsch S, Pasantes J, Wolf A, Bogdanova N, Münch C, Markoff A, et al.: Chromosomal evolution of the PKD1 gene family in primates. *BMC Evol. Biol.* 9: 14, 2009

46. Pinto CS, Raman A, Reif GA, Magenheimer BS, White C, Calvet JP, et al.: Phosphodiesterase Isoform Regulation of Cell Proliferation and Fluid Secretion in Autosomal Dominant Polycystic Kidney Disease. *J. Am. Soc. Nephrol.* 27: 1124–1134, 2016

47. Ahrabi AK, Jouret F, Marbaix E, Delporte C, Horie S, Mulroy S, et al.: Glomerular and proximal tubule cysts as early manifestations of Pkd1 deletion. *Nephrol. Dial. Transplant.* 25: 1067–1078, 2010

48. Karner CM, Chirumamilla R, Aoki S, Igarashi P, Wallingford JB, Carroll TJ: Wnt9b signaling regulates planar cell polarity and kidney tubule morphogenesis. *Nat. Genet.* 41: 793–799, 2009

49. Sutters M, Germino GG: Autosomal dominant polycystic kidney disease: Molecular genetics and pathophysiology. *J. Lab. Clin. Med.* 141: 91–101, 2003

50. Boertien WE, Meijer E, Li J, Bost JE, Struck J, Flessner MF, et al.: Relationship of copeptin, a surrogate marker for arginine vasopressin, with change in total kidney volume and gfr decline in autosomal dominant polycystic kidney disease: Results from the crisp cohort. *Am. J. Kidney Dis.* 61: 420–429, 2013

51. Szabo L, Morey R, Palpant NJ, Wang PL, Afari N, Jiang C, et al.: Statistically based splicing detection reveals neural enrichment and tissue-specific induction of circular RNA during human fetal development. *Genome Biol.* 16: 126, 2015

52. Heyer CM, Sundsbak JL, Abebe KZ, Chapman AB, Torres VE, Grantham JJ, et al.: Predicted Mutation Strength of Nontruncating PKD1 Mutations Aids Genotype-Phenotype Correlations in Autosomal Dominant Polycystic Kidney Disease. *J. Am. Soc.*

Nephrol. 27: 2872–2884, 2016

53. Peral B, Ong ACM, San Millán JL, Gamble V, Rees L, Harris PC: A stable, nonsense mutation associated with a case of infantile onset polycystic kidney disease 1 (PKD1). *Hum. Mol. Genet.* 5: 539–542, 1996

54. Di Mise A, Tamma G, Ranieri M, Centrone M, van den Heuvel L, Mekahli D, et al.: Activation of Calcium-Sensing Receptor increases intracellular calcium and decreases cAMP and mTOR in PKD1 deficient cells. *Sci. Rep.* 8: 5704, 2018

55. Belibi FA, Reif G, Wallace DP, Yamaguchi T, Olsen L, Li H, et al.: Cyclic AMP promotes growth and secretion in human polycystic kidney epithelial cells11See Editorial by Torres, p. 1283. *Kidney Int.* 66: 964–973, 2004

56. Treschan TA, Peters J: The Vasopressin System. *Anesthesiology* 105: 599–612, 2006

57. Liu J, Wess J: Different Single Receptor Domains Determine the Distinct G Protein Coupling Profiles of Members of the Vasopressin Receptor Family. *J. Biol. Chem.* 271: 8772–8778, 1996

58. Ransick A, Lindström NO, Liu J, Zhu Q, Guo J-J, Alvarado GF, et al.: Single-Cell Profiling Reveals Sex, Lineage, and Regional Diversity in the Mouse Kidney. *Dev. Cell* 51: 399-413.e7, 2019

59. Mangos S, Lam PY, Zhao A, Liu Y, Mudumana S, Vasilyev A, et al.: The ADPKD genes pkd1a/b and pkd2 regulate extracellular matrix formation. *Dis. Model. Mech.* 3: 354–365, 2010

60. Tsukiyama T, Kobayashi K, Nakaya M, Iwatani C, Seita Y, Tsuchiya H, et al.: Monkeys mutant for PKD1 recapitulate human autosomal dominant polycystic kidney disease. *Nat. Commun.* 10: 5517, 2019

61. Homan KA, Gupta N, Kroll KT, Kolesky DB, Skylar-Scott M, Miyoshi T, et al.: Flow-

enhanced vascularization and maturation of kidney organoids in vitro. *Nat. Methods* 16: 255–262, 2019

Figure legends

Figure 1. CRISPR-Cas9-mediated generation of *PKD1* mutant iPSCs. (A) Strategy for targeting the human *PKD1* gene. A cassette containing GFP, RFP, and puromycin-resistance gene (Puro) is inserted into exon 15 of *PKD1*. Gray arrowheads, *loxP* sites; black hexagons, insulators; black arrowheads, PCR primers used for panel B; red box, Southern blot probe on a 5' region outside the left arm that hybridizes to pseudogenes other than authentic *PKD1*; S, SphI; B, BamHI; E, EcoRI. (B) PCR screening of homologous recombinants. The primer positions are shown in panel A. (C) Southern blot analysis of wild-type (+/+), heterozygous (+/−), and homozygous (−/−) clones. Genomic DNAs were digested with SphI and EcoRI and hybridized with the probe (red box in panel A). Because the pseudogenes have higher copy numbers, their bands are darker than the authentic *PKD1* band. (D) Western blots of PC1 proteins in iPSCs. An antibody against an N-terminal region of PC1 was used. The asterisk indicates shorter bands, presumably representing truncated PC1 proteins in the heterozygous (+/−) and homozygous (−/−) clones.

Figure 2. *PKD1* mutant nephron organoids do not show cystogenesis. (A) Outline of the induction protocol for nephron organoids from iPSCs through nephron progenitors. Spinal cord was attached to nephron progenitors at day 13 to initiate nephrogenesis. After removing the spinal cord at day 19, the nephron organoids were cultured up to day 25. (B) Flow cytometry analysis at day 13. The percentages of the $ITGA8^{+}/PDGFRA^{-}$ nephron progenitor fraction were determined from five independent experiments (mean ± SEM). (C) Representative bright-field images of nephron organoids at day 25. Scale bars, 200 μm. (D) Representative confocal images of immunostaining at day 25. Nephron segments of the glomeruli ($WT1^{+}$; red), proximal tubules (LTL^{+}; green) and distal tubules ($CDH1^{+}$; blue) were formed in all three genotypes. Scale bars,

200 μm (upper panels) and 50 μm (lower panels).

Figure 3. *PKD1* mutant nephron organoids exhibit cystogenesis upon forskolin treatment. (A) Outline of the induction protocol for nephron organoids with forskolin treatment. After removing the spinal cord at day 19, forskolin was added at a final concentration of 25 μM. (B) Representative bright-field images of nephron organoids at day 25 after treatment with forskolin. Scale bars, 200 μm. (C) Cyst areas in nephron organoids (n=6 per clone). Two clones were analyzed for each genotype. Data are shown as mean ± SEM. **P*<0.05, ***P*<0.01. (D) Representative confocal images of immunofluorescence at day 25. LTL^+ cysts (presumably derived from proximal tubules; asterisks) and $WT1^+$ cysts (presumably derived from glomerular parietal epithelial cells; arrowheads) were detected in organoids, irrespective of the genotypes. Scale bars, 200 μm (upper panels) and 50 μm (lower panels).

Figure 4. *PKD1*$^{-/-}$ UB organoids do not show cystogenesis. (A) Outline of the induction protocol for UB/collecting duct organoids from iPSCs. Wolffian duct progenitors were sorted and reaggregated into spheres at day 6.25. At day 12.5, the spheres were transferred to a branching condition and cultured until day 30. (B) Flow cytometry analysis at day 6.25. The percentages of the $CXCR4^+/KIT^+$ Wolffian duct progenitor fraction were determined from five independent experiments (mean ± SEM). (C) Representative bright-field images of UB organoids at day 18.5 and 30. Scale bars: 200 μm. (D) qPCR analysis of UB markers at day 18.5 (two clones per genotype in three independent experiments). (E) Representative confocal images of immunofluorescence at day 30. The $KRT19^-$ structures in the center of UB organoid were not cysts but occupied by $DAPI^+$ cells. Scale bars, 200 μm (upper panels) and 50 μm (lower panels).

Figure 5. *PKD1* mutant UB organoids exhibit cystogenesis upon forskolin treatment. (A) Outline of the induction protocol for UB organoids with forskolin treatment. At day 18.5, forskolin was added at a final concentration of 25 μM. (B) Time-course bright-field images of UB organoids upon forskolin treatment. Scale bars, 200 μm. (C) Frequency of cyst formation in UB organoids (two clones per genotype; n=4 per clone in five independent experiments). (D) Cyst areas in UB organoids (n=20 per clone). Data are shown as mean ± SEM. **P*<0.05, ***P*<0.01.

Figure 6. *PKD1* mutant cysts express markers for UB epithelia. Confocal images of immunofluorescence in UB organoids at day 24. (A) CALB1 (green) and DBA (red). (B) GATA3 (green) and PAX2 (red). (C) RET (green) and KRT19 (red). (D) RET (green) and AQP2 (red). The asterisks indicate the lumens of cysts. Scale bars, 100 μm (upper panels) and 50 μm (lower panels).

Figure 7. Vasopressin treatment induces cyst formation specifically in *PKD1* mutant UB organoids. (A) qPCR analysis for expression of vasopressin receptors in nephron organoids (NP) at day 19 and UB organoids at day 18.5 (n=2 per genotype in three independent experiments). (B) Confocal images of immunofluorescence for RET (green) and AVPR1A (red) in UB organoids at day 18.5. Scale bars, 100 μm (upper panels) and 50 μm (lower panels). (C) Representative bright-field images of nephron (NP) organoids and UB organoids upon vasopressin treatment (NP, from day 19 to day 31; UB, from day 18.5 to day 30). The black arrowhead shows cyst formation in *PKD1*$^{-/-}$ UB organoids. AVP, vasopressin (300 nM). Scale bars, 200 μm. (D) Frequency of cyst formation upon vasopressin treatment (n=6 per clone in four independent experiments). Data are shown as mean ± SEM. ***P*<0.01.

Figure 8. UB organoids generated from ADPKD patient-derived iPSCs exhibit cystogenesis upon forskolin treatment. (A) Flow cytometry analysis of UB organoids generated from ADPKD patient-derived iPSCs (Patient 4) at day 6.25. Wild-type human iPSCs (201B7) were used as controls. The percentages of the $CXCR4^{+}/KIT^{+}$ Wolffian duct progenitor fraction were determined from three independent induction experiments (mean ± SEM). (B) Representative bright-field images of UB organoids upon forskolin treatment from day 18.5 to day 30. Scale bars, 200 μm. (C) Frequency of cyst formation upon forskolin treatment (n=32 in four independent experiments). Data are shown as mean ± SEM. $^{**}P<0.01$. (D, E) Confocal images of immunofluorescence in UB organoids at day 30 with staining for GATA3 (green) and PAX2 (red) (D) or RET (green) and KRT19 (red) (E). The asterisks indicate the lumens of cysts. Scale bars: 50 μm.

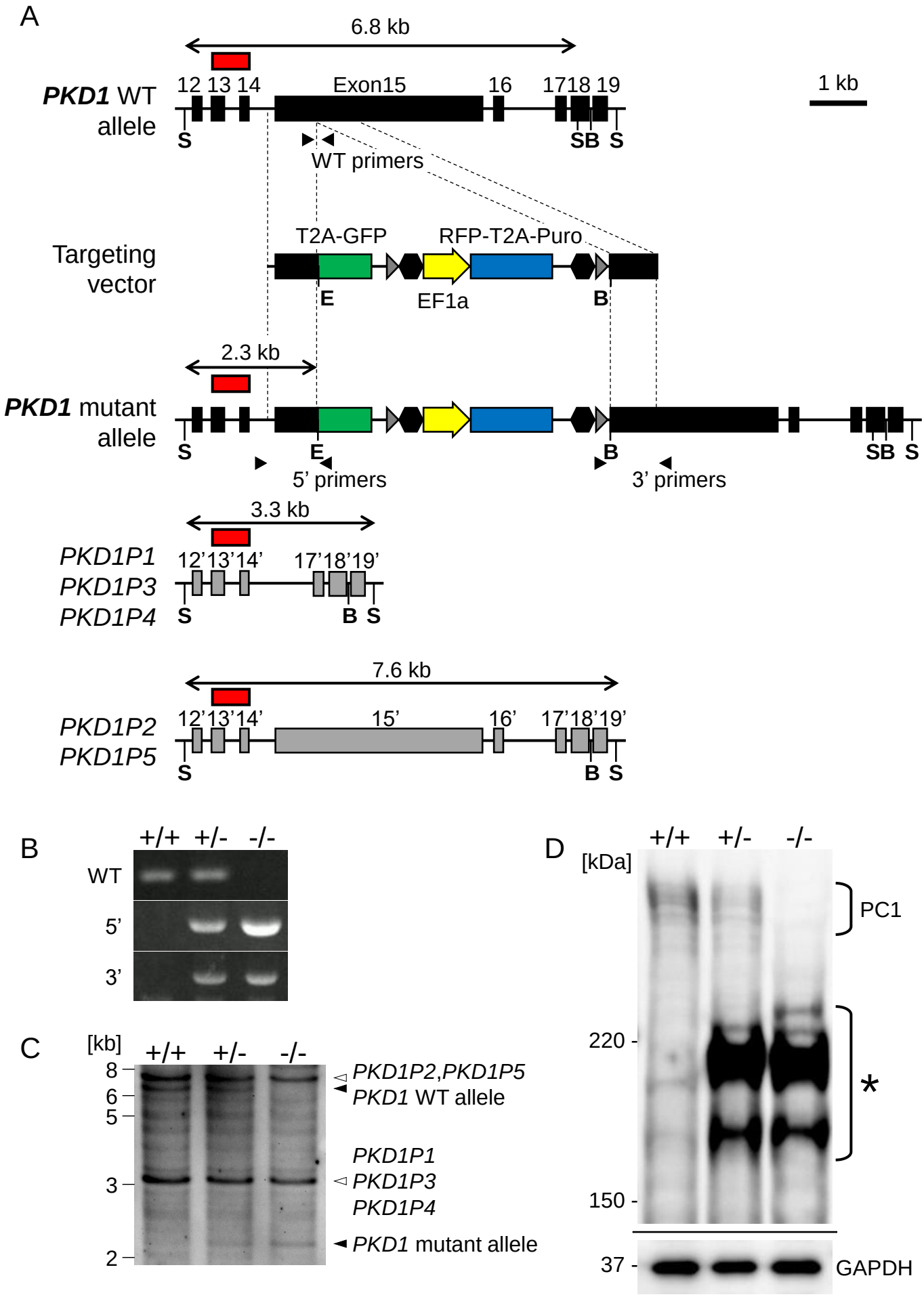
A
6.8 kb
PKD1 WT allele
12 13 14
Exon15
16
17 18 19
1 kb
S
SB S
WT primers
Targeting vector
T2A-GFP
RFP-T2A-Puro
E
EF1a
B
2.3 kb
PKD1 mutant allele
S
E
B
SB S
5' primers
3' primers
3.3 kb
PKD1P1
PKD1P3
PKD1P4
12'13'14'
17'18'19'
S
B S
7.6 kb
PKD1P2
PKD1P5
12'13'14'
15'
16'
17'18'19'
S
B S
B
+/+ +/- -/-
WT
5'
3'
C
[kb]
+/+ +/- -/-
8
6
5
3
2
PKD1P2,PKD1P5
PKD1 WT allele
PKD1P1
PKD1P3
PKD1P4
PKD1 mutant allele
D
+/+ +/- -/-
[kDa]
PC1
220
150
*
37
GAPDH

A

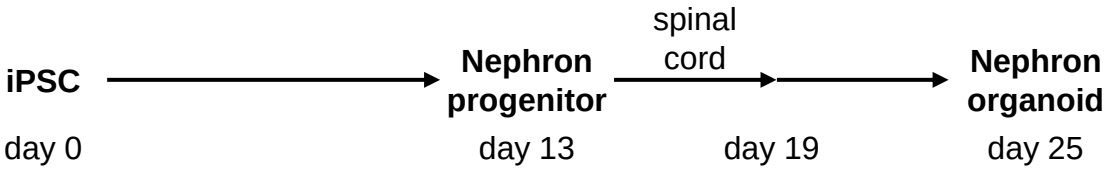
iPSC
Nephron progenitor
spinal cord
Nephron organoid
day 0
day 13
day 19
day 25

B

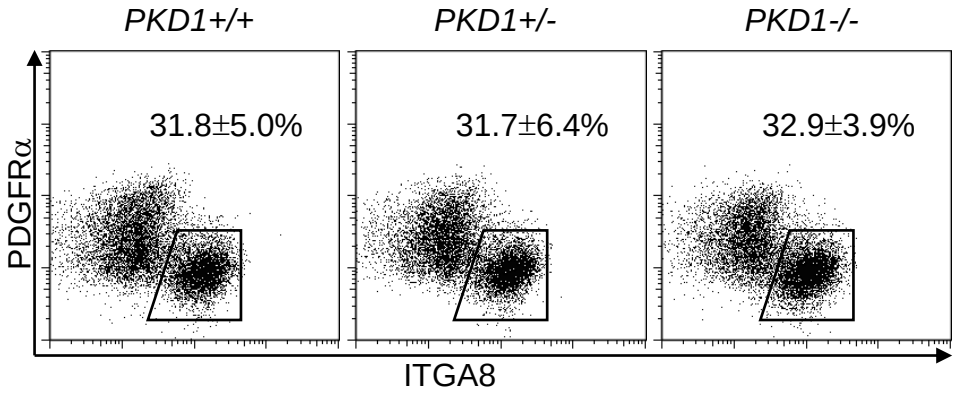
PKD1+/+
PKD1+/-
PKD1-/-
31.8±5.0%
31.7±6.4%
32.9±3.9%
PDGFRα
ITGA8

C

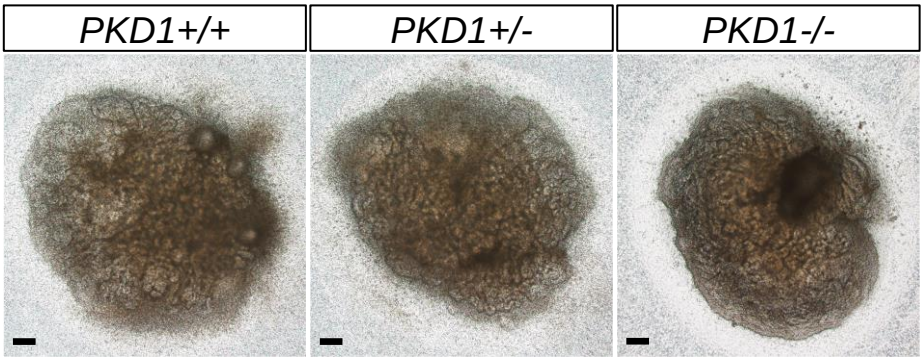
PKD1+/+
PKD1+/-
PKD1-/-

D

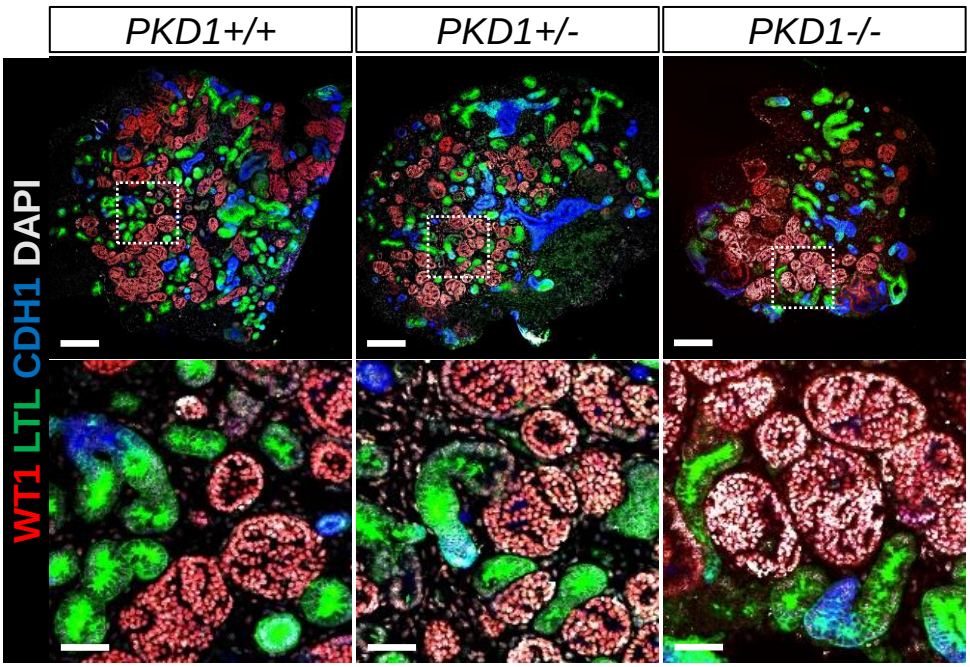
PKD1+/+
PKD1+/-
PKD1-/-
WT1 LTL CDH1 DAPI

A

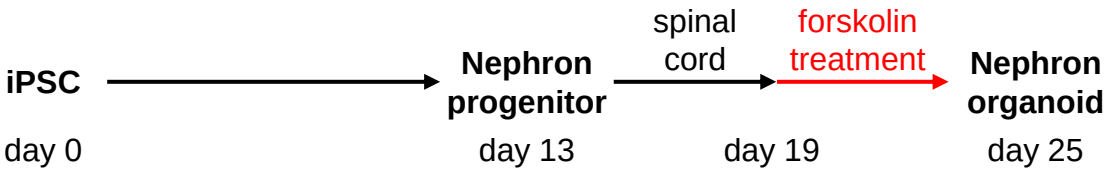
iPSC
Nephron progenitor
spinal cord
forskolin treatment
Nephron organoid
day 0
day 13
day 19
day 25

B

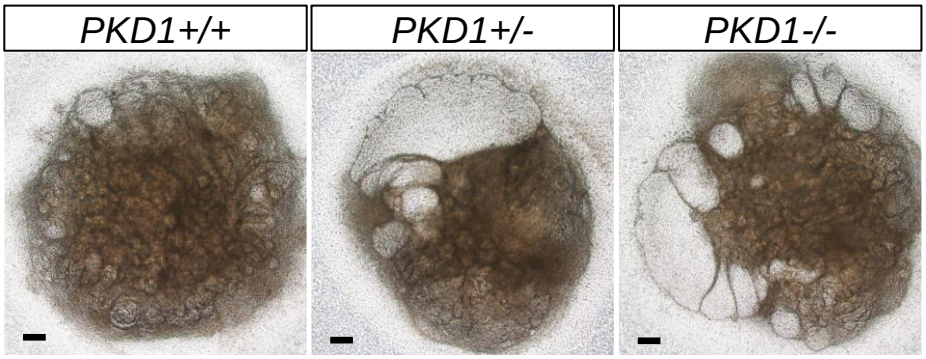
PKD1+/+
PKD1+/-
PKD1-/-

C

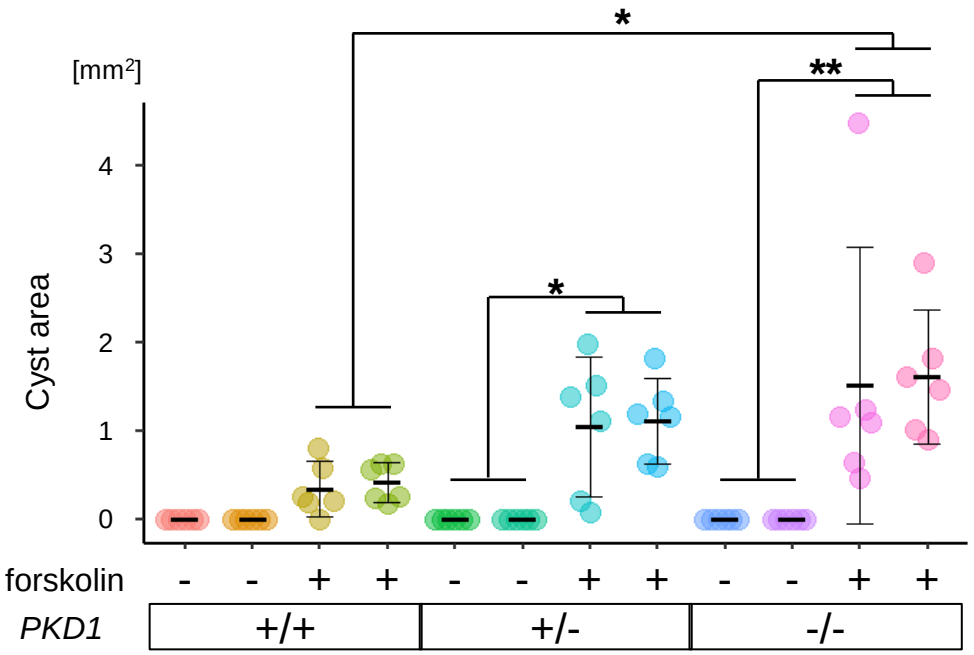
[mm²]
Cyst area
0
1
2
3
4
*
**
*
forskolin - - + + - - + + - - + +
PKD1 +/+ +/- -/-

D

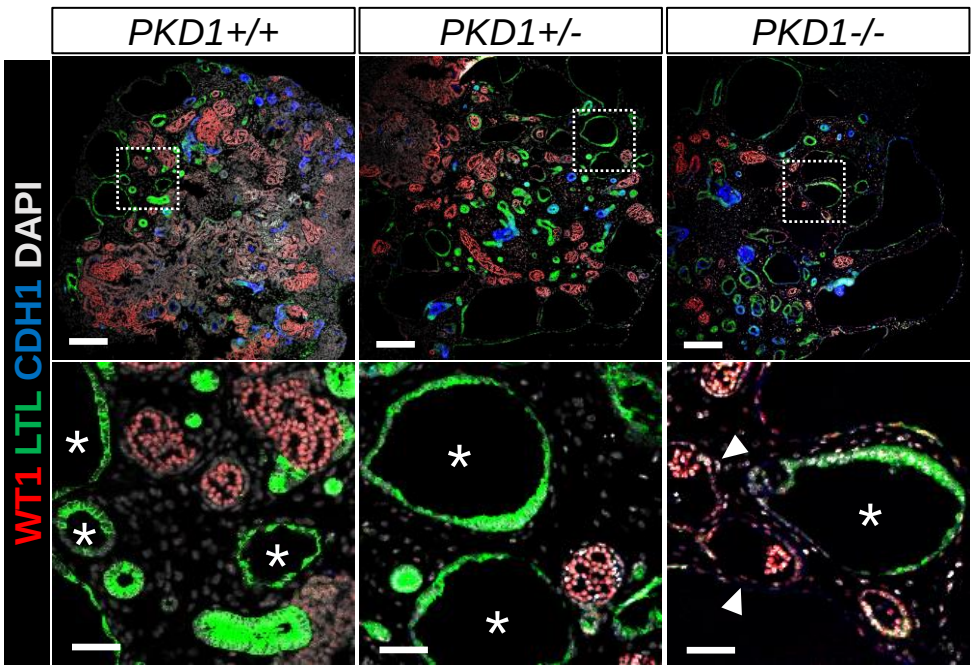
PKD1+/+
PKD1+/-
PKD1-/-
WT1 LTL CDH1 DAPI

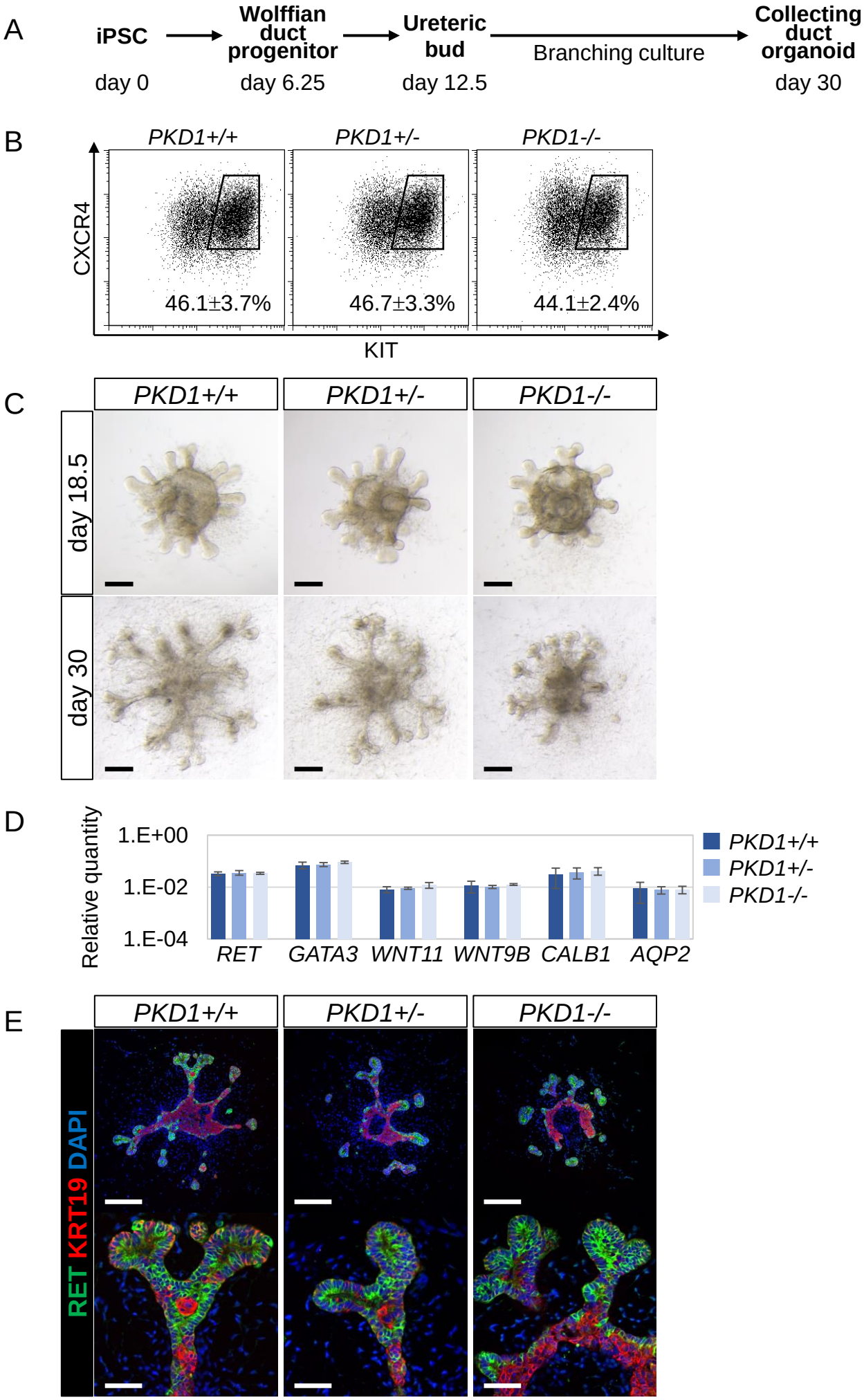
A
iPSC
day 0
Wolffian duct progenitor
day 6.25
Ureteric bud
day 12.5
Branching culture
Collecting duct organoid
day 30
B
PKD1+/+
PKD1+/-
PKD1-/-
CXCR4
KIT
46.1±3.7%
46.7±3.3%
44.1±2.4%
C
PKD1+/+
PKD1+/-
PKD1-/-
day 18.5
day 30
D
Relative quantity
1.E+00
1.E-02
1.E-04
RET
GATA3
WNT11
WNT9B
CALB1
AQP2
PKD1+/+
PKD1+/-
PKD1-/-
E
PKD1+/+
PKD1+/-
PKD1-/-
RET KRT19 DAPI

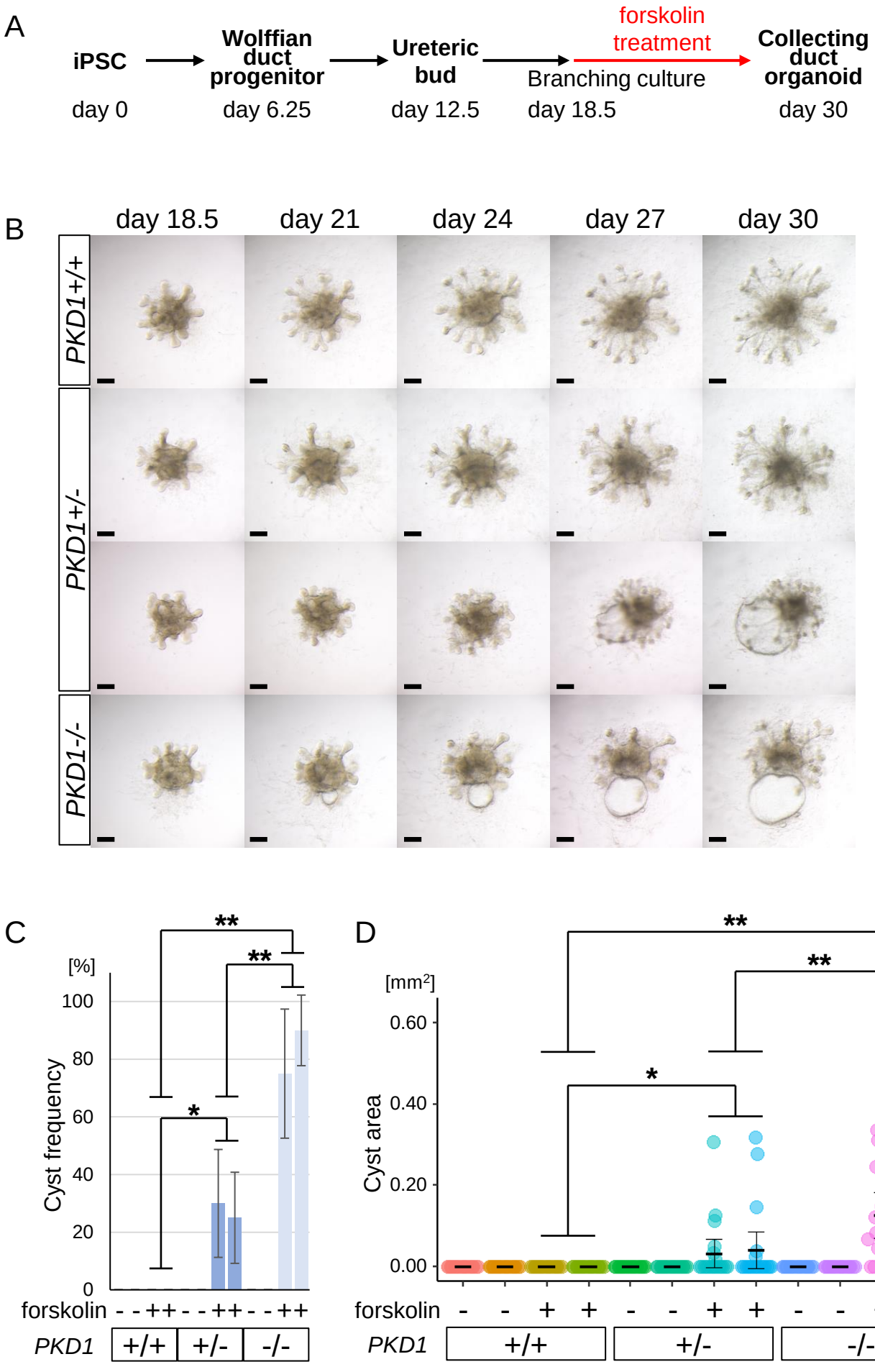
A
iPSC
day 0
Wolffian duct progenitor
day 6.25
Ureteric bud
day 12.5
Branching culture
day 18.5
forskolin treatment
Collecting duct organoid
day 30
B
day 18.5
day 21
day 24
day 27
day 30
PKD1+/+
PKD1+/-
PKD1-/-
C
[%]
Cyst frequency
100
80
60
40
20
0
**
**
*
forskolin - - ++ - - ++ - - ++
PKD1 +/+ +/- -/-
D
[mm²]
Cyst area
0.60
0.40
0.20
0.00
**
**
*
forskolin - - + + - - + + - - + +
PKD1 +/+ +/- -/-

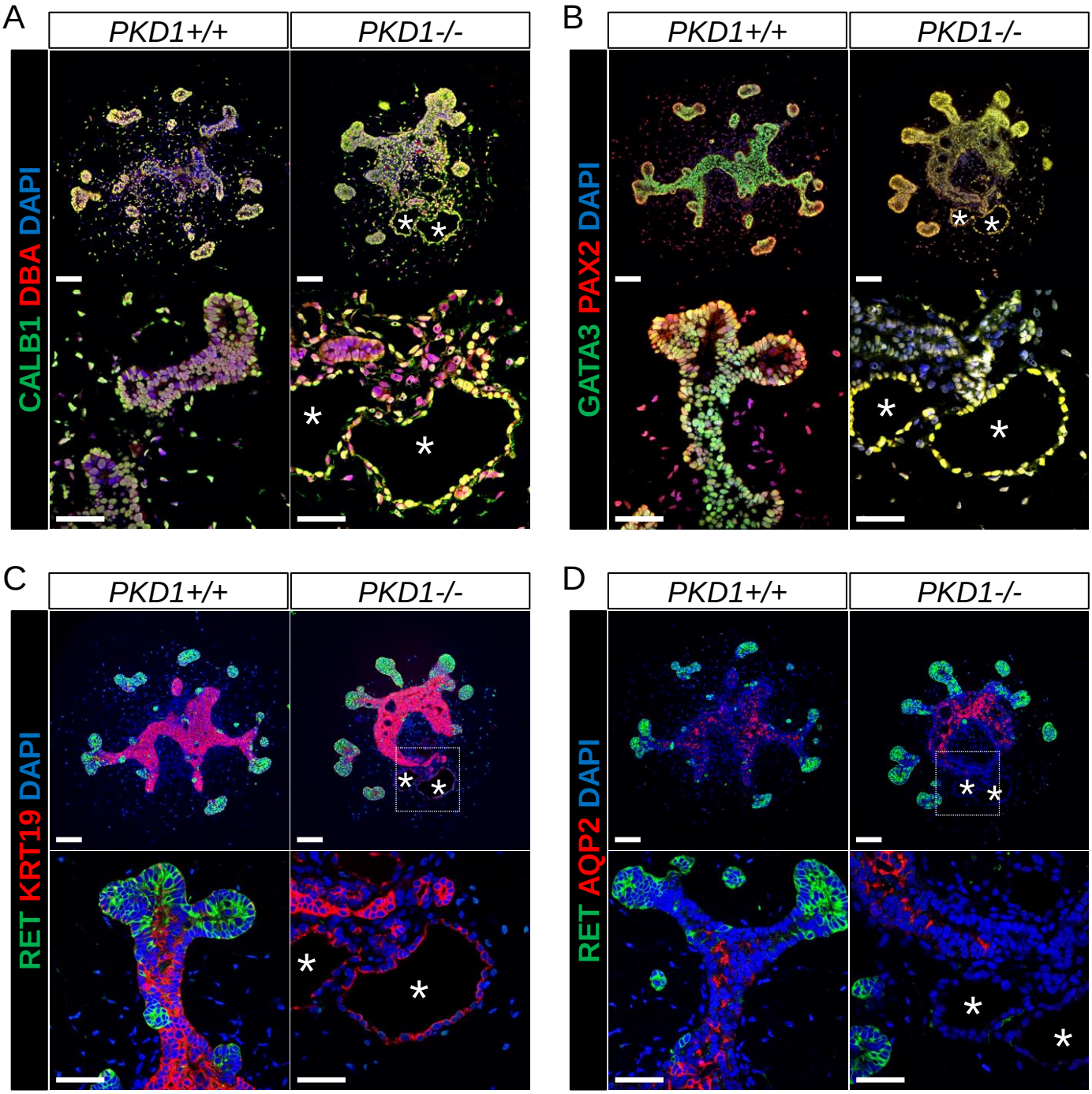
A
PKD1+/+
PKD1-/-
CALB1 DBA DAPI
B
PKD1+/+
PKD1-/-
GATA3 PAX2 DAPI
C
PKD1+/+
PKD1-/-
RET KRT19 DAPI
D
PKD1+/+
PKD1-/-
RET AQP2 DAPI

A

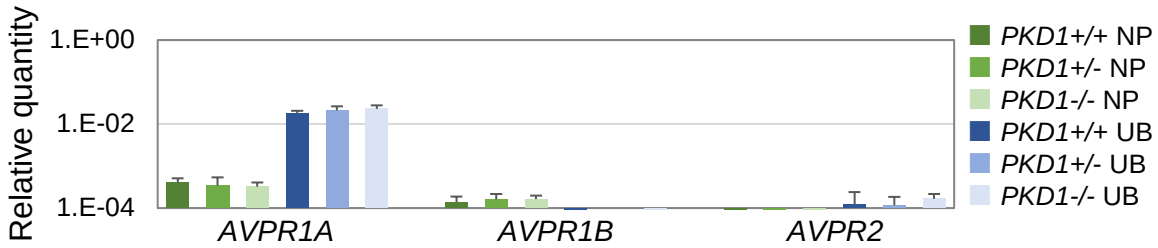
Relative quantity
1.E+00
1.E-02
1.E-04
AVPR1A
AVPR1B
AVPR2
PKD1+/+ NP
PKD1+/- NP
PKD1-/- NP
PKD1+/+ UB
PKD1+/- UB
PKD1-/- UB

B

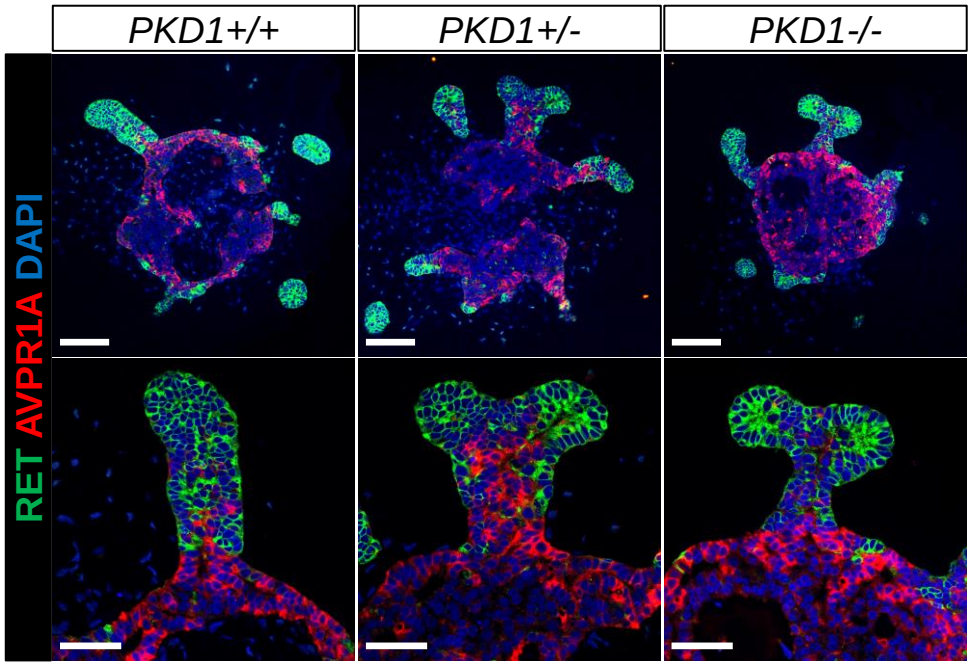
PKD1+/+
PKD1+/-
PKD1-/-
RET AVPR1A DAPI

C

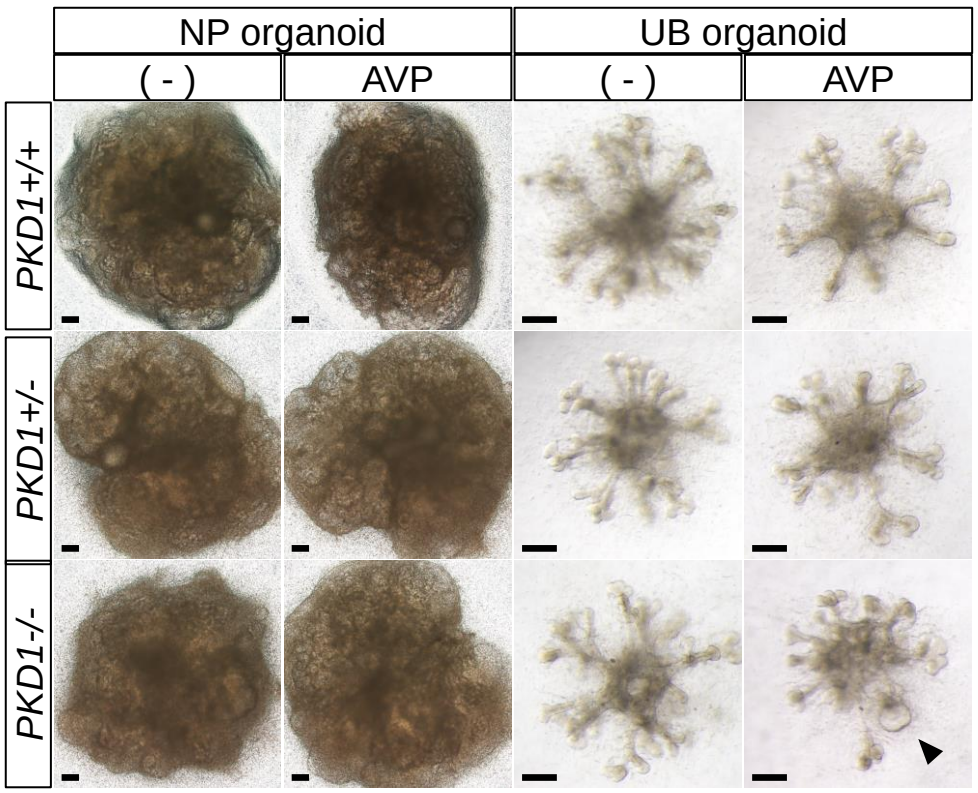
NP organoid
UB organoid
(-)
AVP
(-)
AVP
PKD1+/+
PKD1+/-
PKD1-/-

D

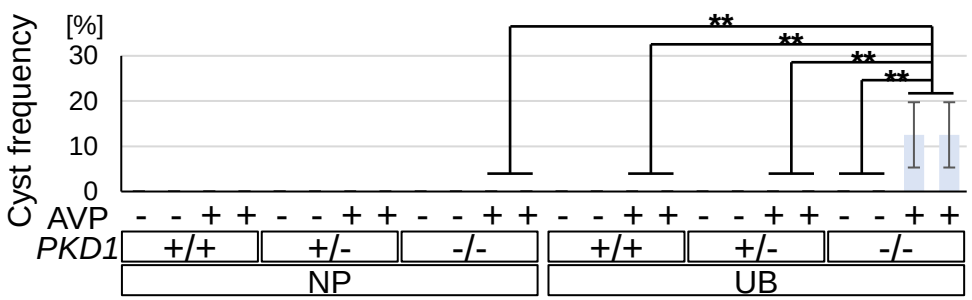
Cyst frequency
[%]
30
20
10
0
**
**
**
**
AVP
PKD1
+/+
+/-
-/-
+/+
+/-
-/-
NP
UB

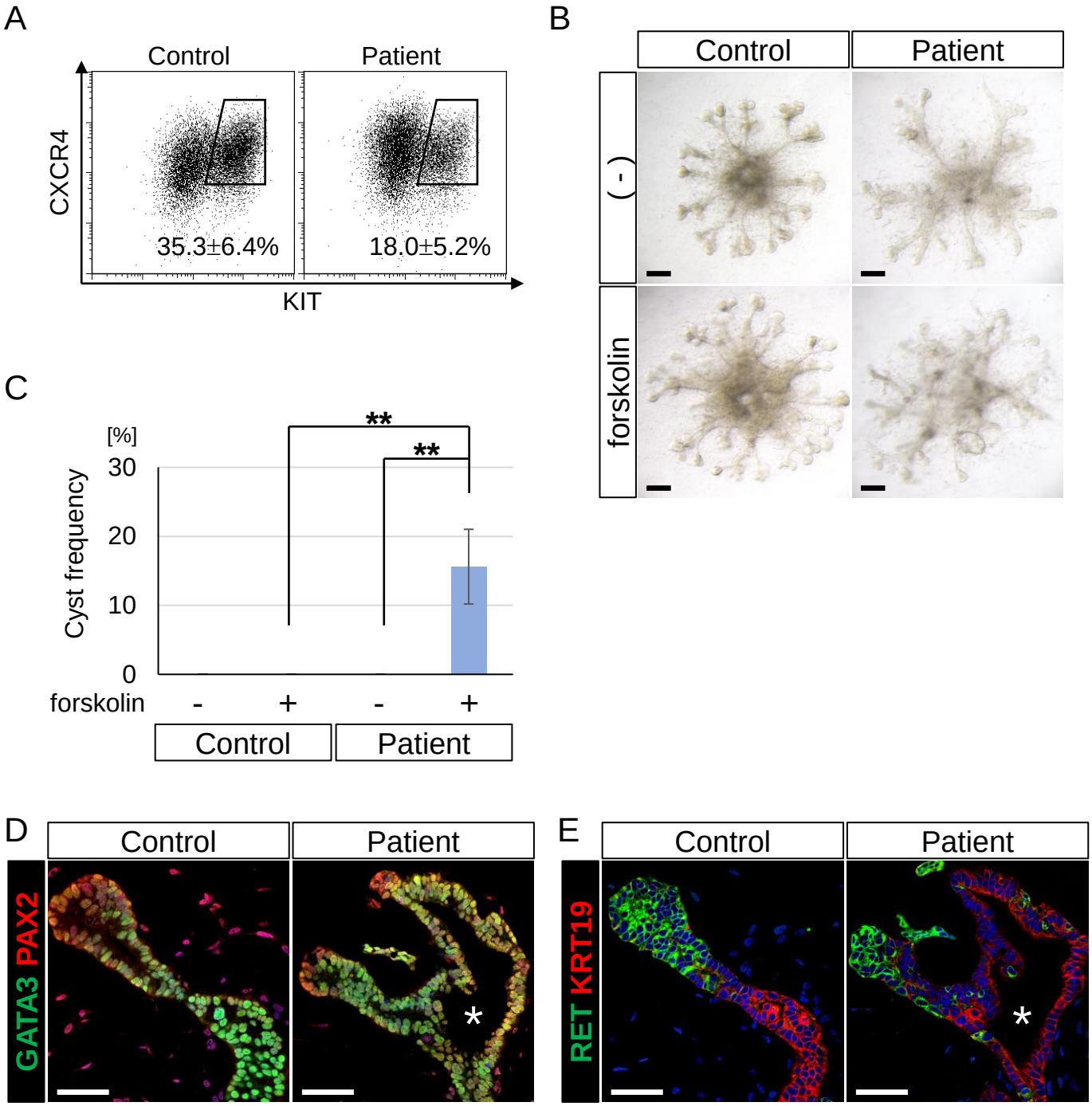
A
Control
Patient
CXCR4
35.3±6.4%
18.0±5.2%
KIT
B
Control
Patient
(-)
forskolin
C
[%]
30
20
10
0
Cyst frequency
**
**
forskolin
-
+
-
+
Control
Patient
D
Control
Patient
GATA3 PAX2
*
E
Control
Patient
RET KRT19
*

Supplemental Information

PKD1-dependent renal cystogenesis in human induced pluripotent stem cell-derived ureteric bud organoids

Shohei Kuraoka, Shunsuke Tanigawa, Atsuhiro Taguchi, Akitsu Hotta, Hitoshi Nakazato, Kenji Osafune, Akio Kobayashi, Ryuichi Nishinakamura

SUPPLEMENTAL TABLE OF CONTENTS

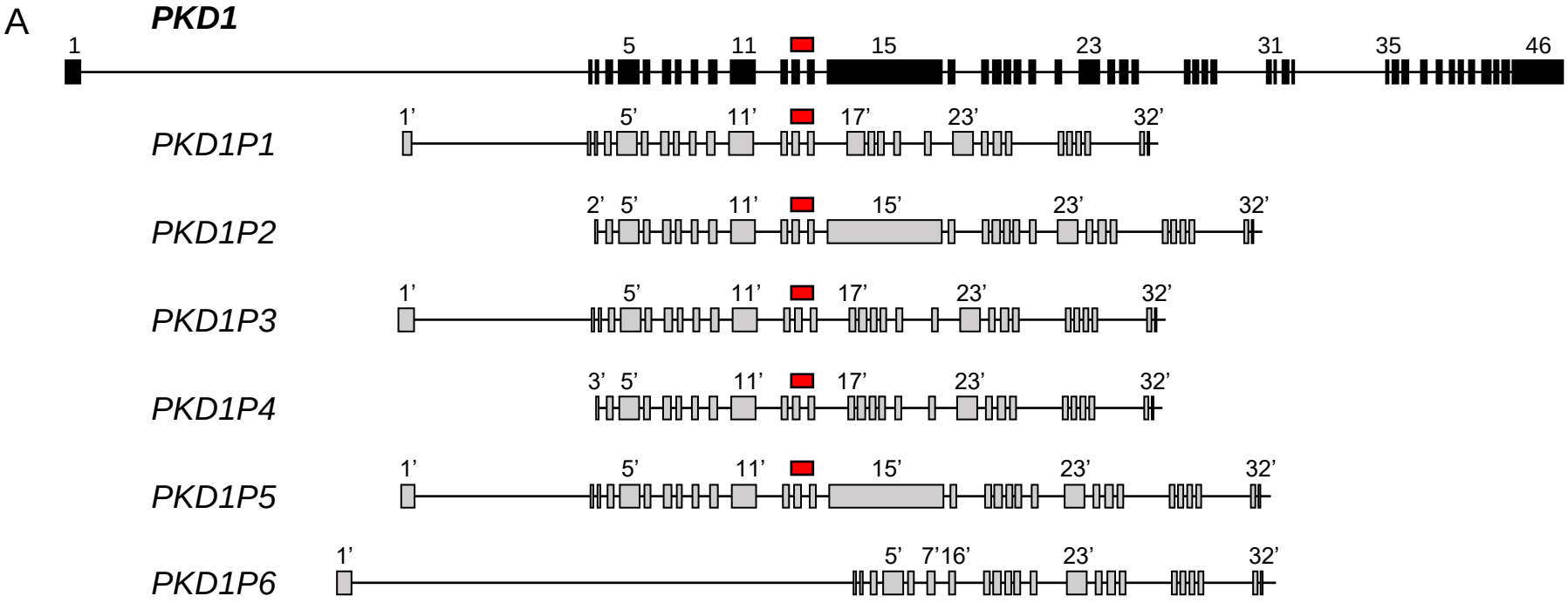

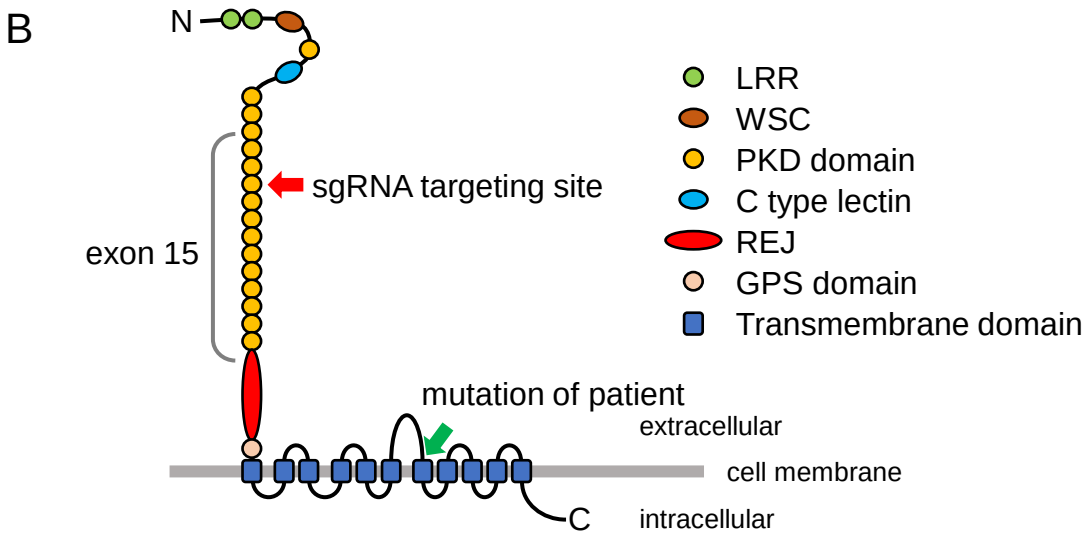

Supplemental Figure 1. Schematic illustration of the *PKD1* locus and PC1 protein. (A) Genomic structures of *PKD1* and the pseudogenes. The positions of *PKD1* exons are shown as black boxes. The numbered gray boxes in the pseudogenes show similar sequences to the corresponding authentic exons. The red boxes indicate the Southern blot probe. (B) Structure of PC1 protein. The red arrow indicates the sgRNA targeting site. The green arrow indicates the mutation site in Patient 4 (G3818R). LRR, leucine rich repeats; WSC, cell wall integrity and stress response component 1; PKD, polycystic kidney disease; REJ, receptor for egg jelly; GPS, G-protein-coupled receptor proteolytic site; N, N-terminus; C, C-terminus

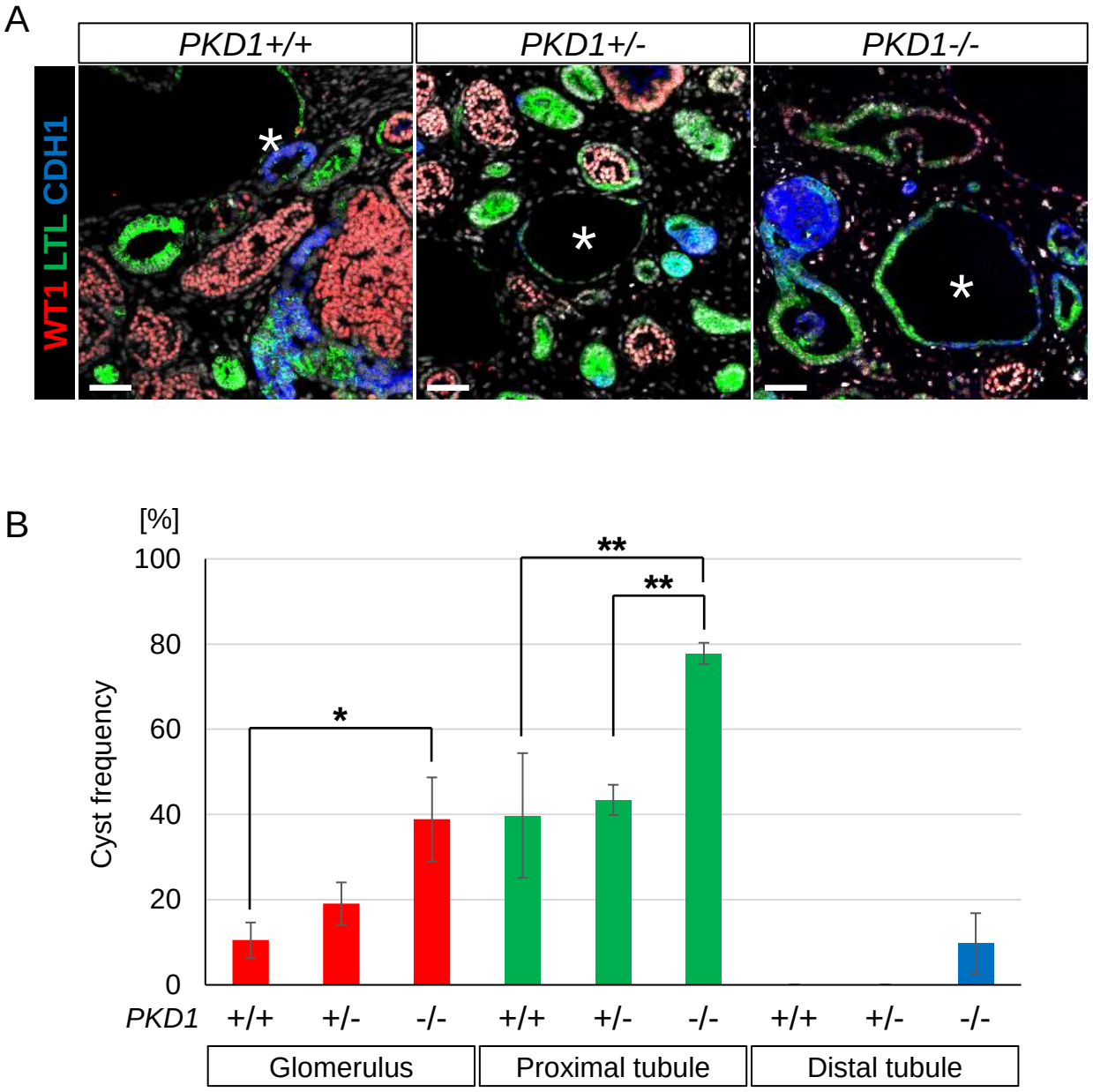

Supplemental Figure 2. The majority of cysts are formed from glomeruli and proximal tubules in nephron organoids. (A) Confocal images of immunofluorescence in nephron organoids treated with forskolin at day 25. WT1 (red), LTL (green), and CDH1 (blue). The asterisks indicate cysts expressing both CDH1 and LTL. Scale bars, 50 μm. (B) Frequency of cyst formation in each segment of nephron organoids. Data are shown as mean ± SEM. **P*<0.05, ***P*<0.01.

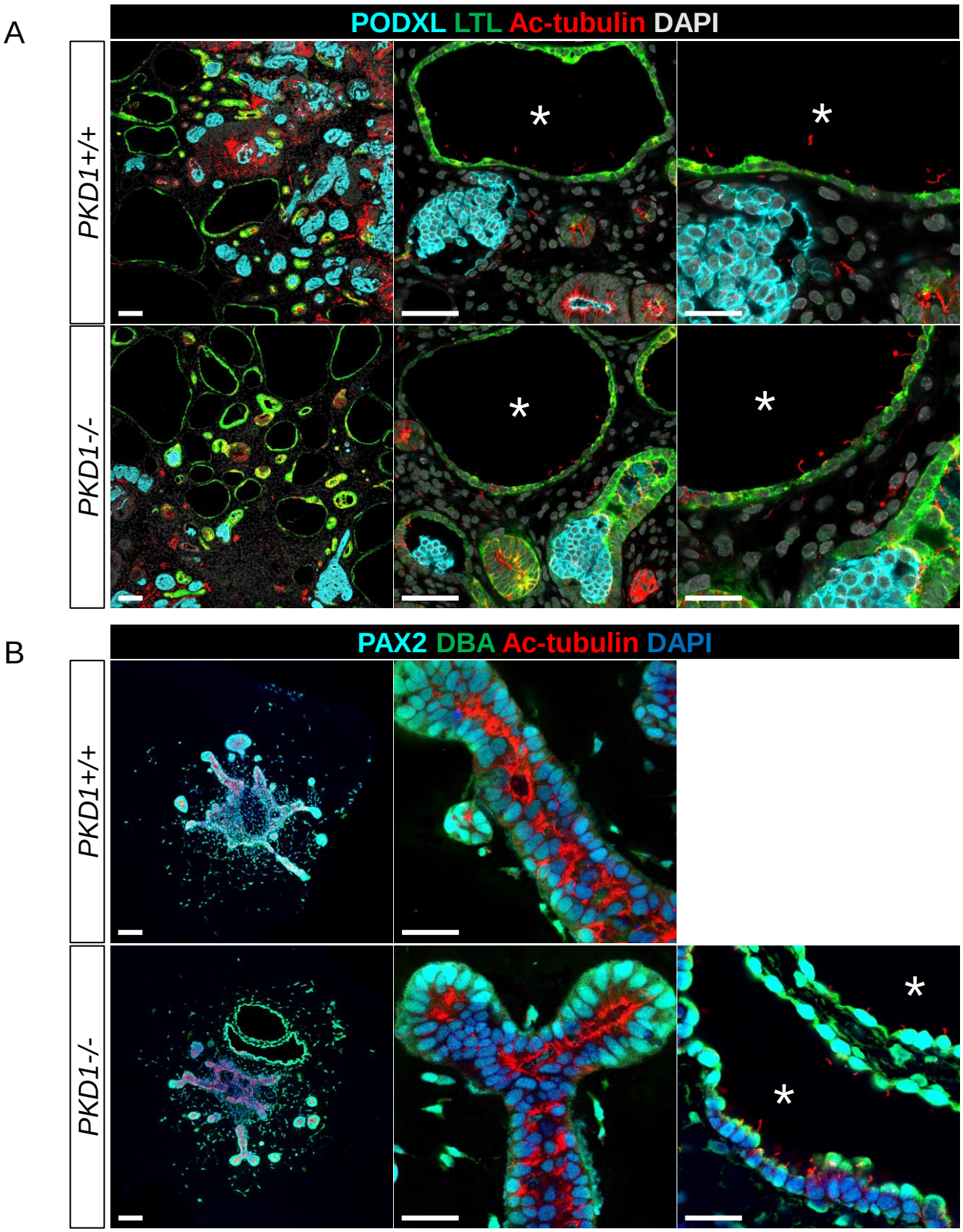

Supplemental Figure 3. Both nephron and UB organoid cysts express primary cilia marker at the luminal side. Confocal images of immunofluorescence in nephron organoids treated with forskolin at day 25. (A) Podocalyxin (PODXL; cyan), LTL (green), and acetylated α-tubulin (Ac-tubulin; red). (B) PAX2 (cyan), DBA (green), and acetylated α-tubulin (Ac-tubulin; red). The asterisks indicate the lumens of cysts. Scale bars, 100 μm (left panels) and 25 μm (middle and right panels).

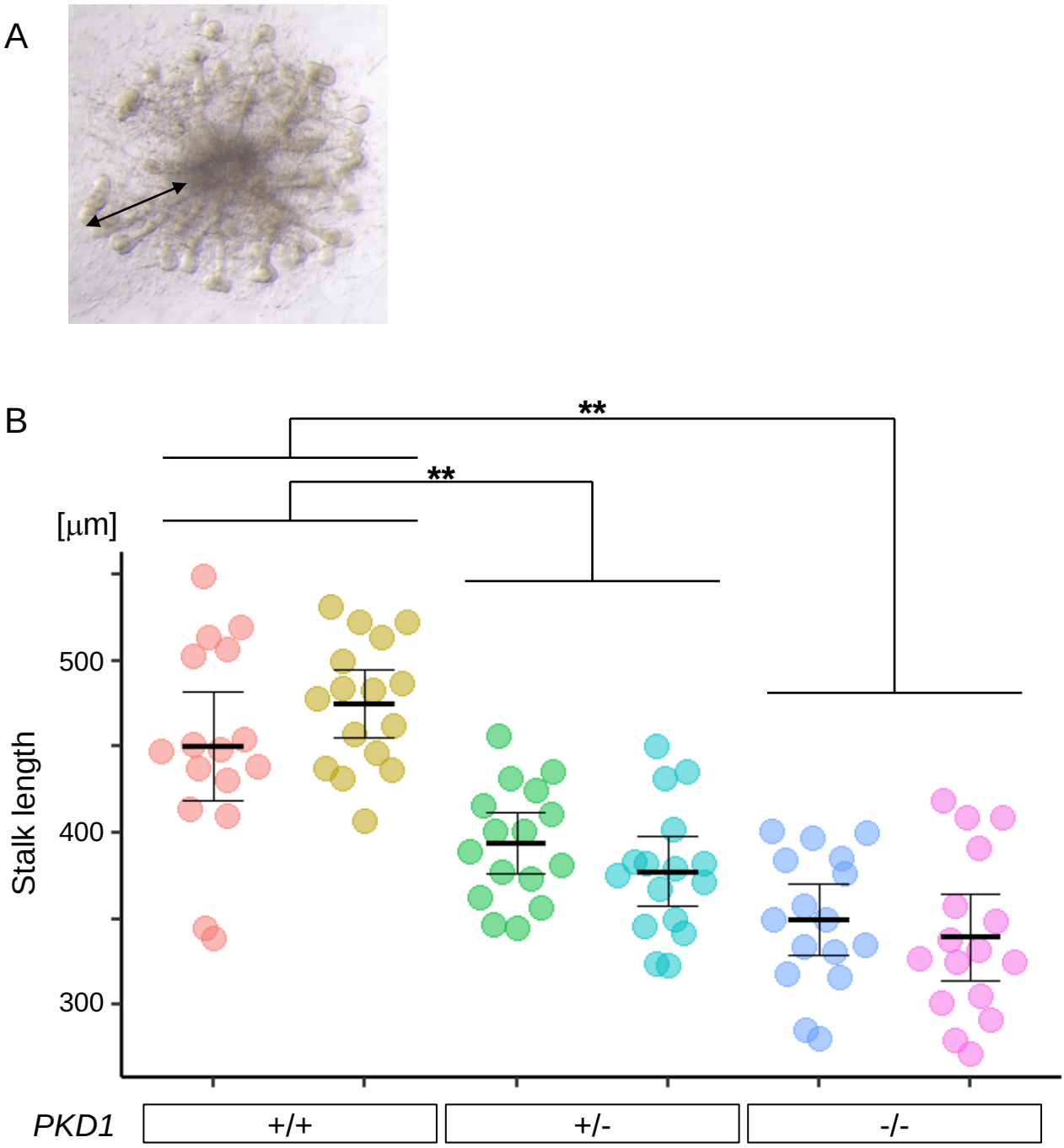

Supplemental Figure 4. *PKD1*$^{-/-}$ UB organoids exhibited shorter stalks in the absence of forskolin. (A) Representative bright-field images of UB organoids at day 30. The lengths of the top four longest stalks in each organoid (double arrow) were averaged and plotted in panel (B). (B) Stalk lengths in UB organoids (n=16 per clone). Two clones were analyzed for each genotype. Data are shown as mean ± SEM. $^{**}P<0.01$.

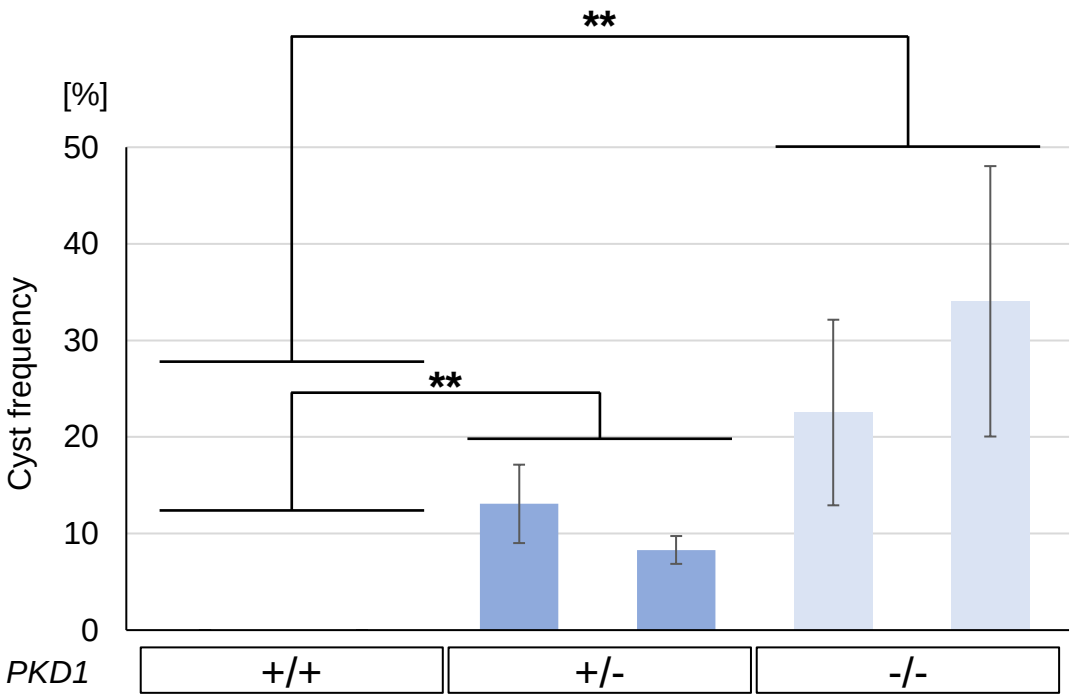

Supplemental Figure 5. *PKD1* mutant UB organoids exhibit cystogenesis upon forskolin treatment. Frequency of cysts relative to the total numbers of ureteric stalks emanating from the center of each UB organoid (n=12 per clone). Two clones per genotype were analyzed. Data are shown as mean ± SEM. ***P*<0.01.

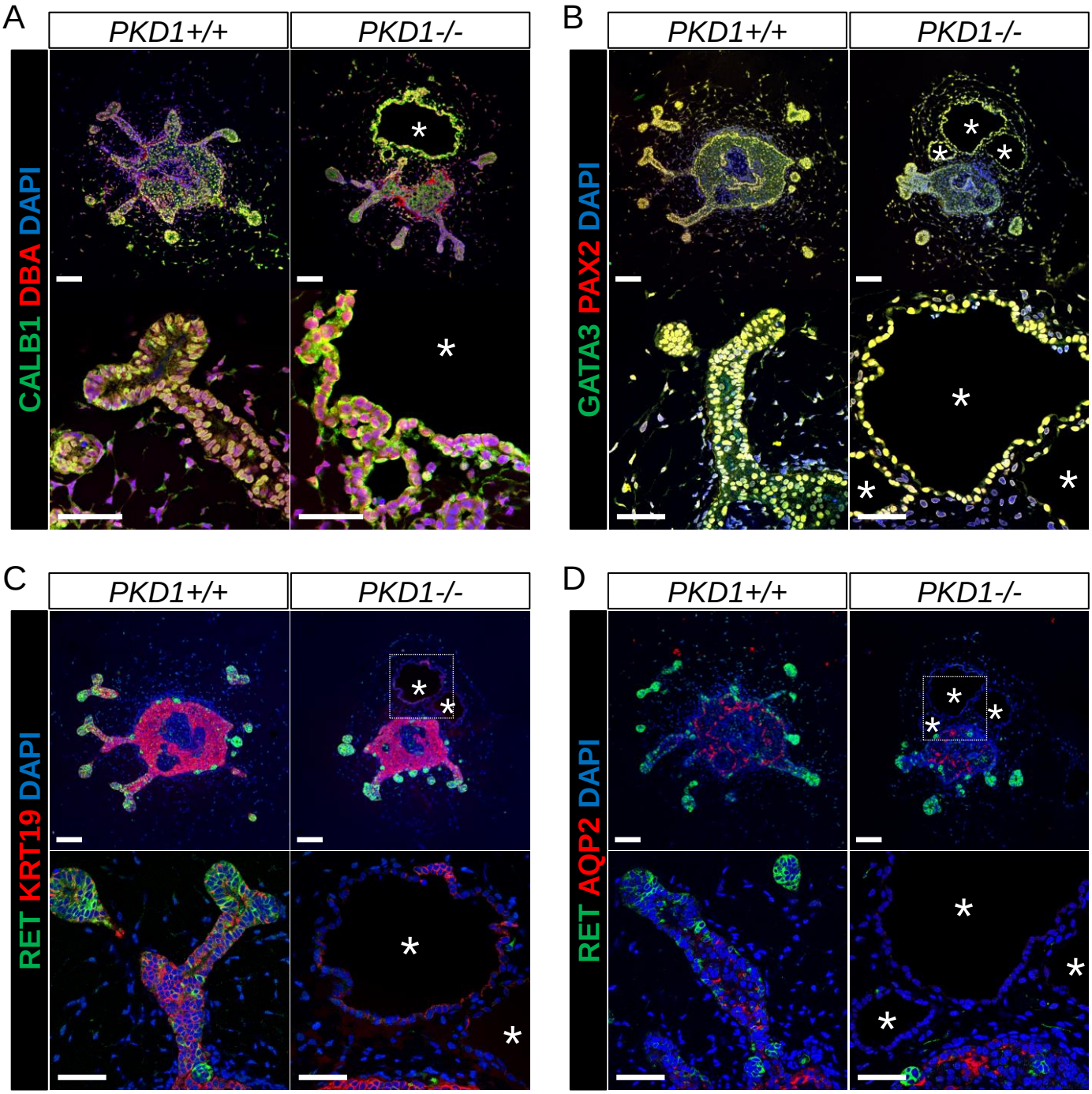

Supplemental Figure 6. UB markers are expressed in the cysts of *PKD1*$^{-/-}$ UB organoids at day 30. Confocal images of immunofluorescence in UB organoids at day 30. (A) CALB1 (green) and DBA (red). (B) GATA3 (green) and PAX2 (red). (C) RET (green) and KRT19 (red). The KRT19^{-} structures in the center of UB organoid were not cysts but occupied by DAPI^{+} cells. (D) RET (green) and AQP2 (red). The asterisks indicate the lumens of cysts. Scale bars, 100 μm (upper panels) and 50 μm (lower panels).

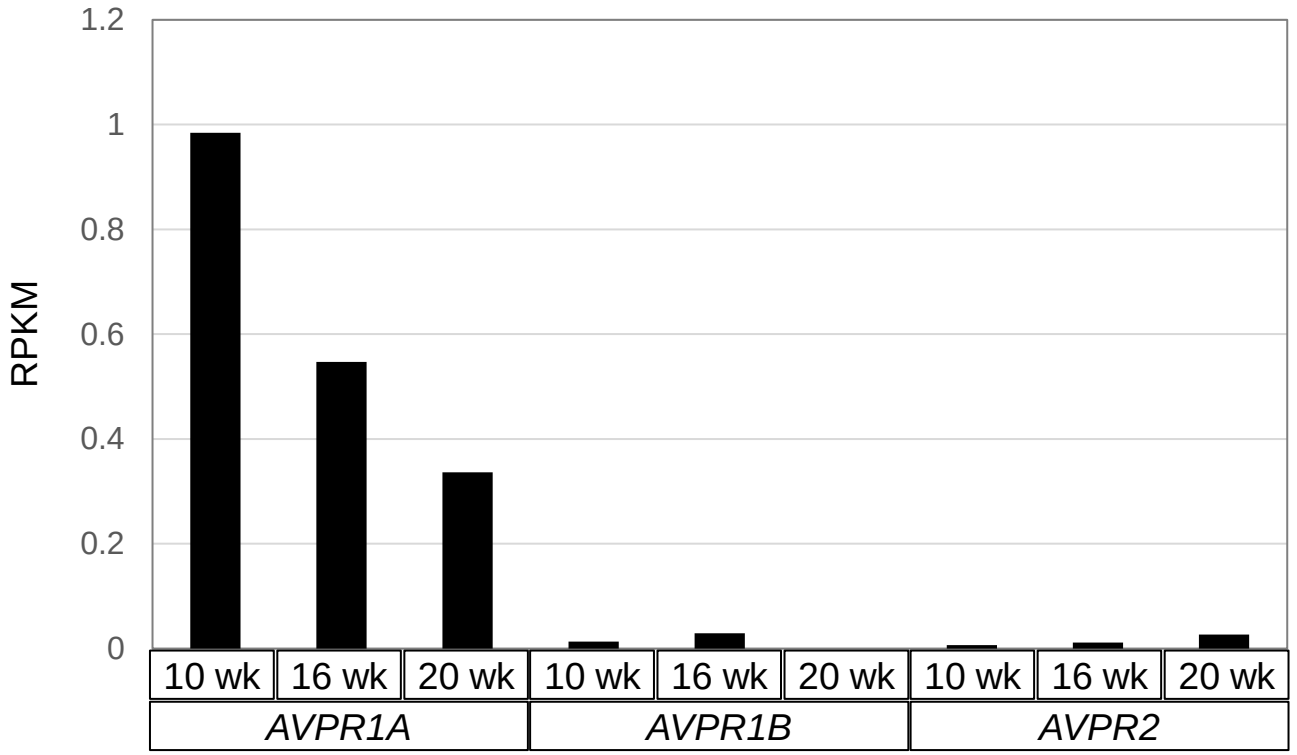

Supplemental Figure 7. *AVPR1A* is dominantly expressed in the human embryonic kidney. Expression of *AVPR1A*, *AVPR1B*, and *AVPR2* in the human embryonic kidney at 10, 16, and 20 weeks of gestation. Data were obtained from the BioProject deposited in NCBI (GEO: GSE64283). RPKM, reads per kilobase of exon per million mapped sequence reads.

Supplemental Table 1. Primer Sequences

Purpose	Primer name	5'-Sequence-3'
Construction of PKD1-sgRNA plasmid	PKD1-sgRNA-Target-fwd	GAGACCACTTGGATCC**GCTCCTCCAACACG ACCGTGCGG**GTTTTAGAGCTAGAAATAGCA
	sgRNA-Universal-rev	GCCCGGGTTTGAATTCAAAAAAAGCACCGA CTCGGTGCCACTTTTTCAAGTTGATAACGGA CTAGCCTTATTTTAACTTGCTATTTCTAGCTC
To amplify 5' arm of the targeting vector	5' arm-fwd	GAATTCAGCCCTCAGTGCTGCTAC
	5' arm-rev	GAATTCCACGGTCGTGTTGGAGGAGCCATC CCCG
To amplify 3' arm of the targeting vector	3' arm-fwd	GGATCCGGGGGTGCCCGACGGTGACACAC AACTTCACGCGG
	3' arm-rev	GCATGCGAAGGTGTAAGAGATGGTAG
To check mutagenic effect of CRISPR, To check target sequence	Target-fwd	CAGATGCTGGTGAAGTAATG
	Target-rev	AGGTGCTGCGCGTTGAAC
Screening 5' recombination by PCR	Left-fwd	AAGCTGGGCCCCTGAACTGCG
	Left-rev	CCACCAGCTCGAACTCCA
Screening 3' recombination by PCR	Right-fwd	TTCAGAGGAAAGCGATCCCG
	Right-rev	AGCCCACCTCGTTCTCAGCC
To amplify DIG probe for southern blot	DIG probe-fwd	TCACCGTGAACTACAACGTA
	DIG probe-rev	TGGGGCAGCGTAGGTGTGCA
Quantitative RT-PCR analysis	RET-fwd	TGCAATGCTGGAAGCAGGAG
	RET-rev	ACGCCGCAAGGTCCAAGTAG
	GATA3-fwd	CGAGATGGCACGGGACACTA
	GATA3- rev	TGGTCTGACAGTTCGCACAGG
	WNT11-fwd	ATGTGCGGACAACCTCAGCTAC
	WNT11-rev	GATGGAGCAGGAGCCAGACA
	WNT9B-fwd	GTGACAACCTCAAGTACAGCACCAA
	WNT9B-rev	CTGATACGCCATGGCACTTACAC
	CALB1-fwd	GATACTGACCACAGTGGCTTCATAG
	CALB1-rev	GCCATCTCAGTTAATTCCAGCTTC
	AQP2-fwd	CCACTTGGCCTCACTACCAGAA
	AQP2-rev	CACATCCATGCTGGGCTCATA
	AVPR1A-fwd	GATCCGCACGGTGAAGATGA
	AVPR1A-rev	AACCCAGTAATGCAGTGATGGTGA
	AVPR1B-fwd	TCCGAACAGTGAAGATGACCTTTG
	AVPR1B-rev	GCTGTTGAAGCCCATGTAGATCC
	AVPR2-fwd	TCCTGAACCCAACCTAGATCCT
	AVPR2-rev	GACACGCTGCTGCTGAAAG

Supplemental Methods

Southern blot analysis

The digoxygenin-labeled probes for Southern blot analysis were amplified using a PCR Dig Probe Synthesis Kit (Roche; #11636090910) with DIG probe-fwd and DIG probe-rev primers. The genomic DNA of each iPSC clone was digested with EcoRI and SphI overnight at 37° C, and electrophoresed in a 0.7% agarose gel. The DNA fragments were denatured with alkali salt solution, transferred and cross-linked to a nylon membrane (Roche; #11417240001), and hybridized with the digoxygenin-labeled probes overnight at 42° C in DIG Easy Hyb solution (Roche; # 11603558001). After washing, the hybridized DNA fragments were detected using Anti-Digoxigenin-AP Fab fragments (Roche; #11093274910) followed by CDP-Star (Roche; #12041677001).

Western blot analysis

Scraped iPSCs of each genotype were lysed in 200 µl of lysis buffer containing 25 mM HEPES-KOH (pH 7.8), 150 mM KCl, 1 mM $MgCl_2$, 1% Triton X-100, 1% sucrose, proteinase inhibitor cocktail (Roche; #5892791001), and phosphatase inhibitor cocktail (Roche; #04906845001), and homogenized on ice three times for 15 s each using Ultrasonic processor (Cole-Parmer; #GE70). The protein concentrations were determined using an Rc-protein assay kit and a BSA standard (Bio-Rad Laboratories; #5000121JA). Protein samples (30 µg each) were denatured in 4× LDS sample buffer (Invitrogen; #NP0007) at 70° C for 10 min and resolved in NuPAGE 3%–8% Tris-Acetate (TA) gel (Invitrogen; #EA03752) with TA Running buffer (Invitrogen; #LA0041). The separated proteins were transferred to PVDF membranes (Millipore; #IPVH304F0) for 3 h, blocked with 5% non-fat dry milk in Tris-buffered saline containing 0.1% Triton X-100 (TBST), and incubated overnight at 4° C with an anti-PC1 antibody (Santa Cruz Biotechnology; sc-130554). As the loading control, same protein samples (0.5 µg each) were resolved in NuPAGE 4%–12% Bis-Tris gel (Invitrogen; #NP0336) with MOPS Running buffer (Invitrogen; #NP0001). The separated proteins were transferred to PVDF membranes for 2 h, blocked with 5% non-fat dry milk in TBST, and incubated overnight at 4° C with an anti-GAPDH antibody (Invitrogen; #NP0336). The membranes were then washed with TBST, incubated with an HRP-conjugated secondary antibody (KPL; #474-1802), and visualized using the ECL Select Western Blotting Detection reagent (GE Healthcare; #RPN2235) according to the manufacturer's instructions.

Flow cytometry

Flow cytometry was done as described[1]. Induced nephron progenitors at day 13 and Wolffian duct progenitors at day 6.25 were dissociated by incubation with 0.25% trypsin/EDTA for 6 min at 37° C.

After blocking in normal mouse serum (Thermo Fisher Scientific), staining was carried out in a buffer comprising 1% bovine serum albumin, 1× Hank's balanced saline solution, and 0.035% $NaHCO_3$. The antibodies used for staining of nephron progenitors were phycoerythrin-conjugated anti-PDGFRA (Biolegend; #323506), biotinylated anti-ITGA8 (R&D Systems; #BAF4076) detected by allophycocyanin-conjugated streptavidin (Biolegend; #554061). The antibodies used for staining of Wolffian duct progenitors were allophycocyanin-conjugated anti-human CXCR4 (Biolegend; #306510) and phycoerythrin-conjugated anti-human KIT (Biolegend; #313204).

Immunohistochemical analysis

Organoids were fixed in 10% formalin, embedded in paraffin, and cut into 6-μm sections. Antigen retrieval in citrate buffer was performed before staining. Staining was perfomed by biotinylated LTL (Vector Laboratories; #B-1325), biotinylated DBA (Vector Laboratories; #B-1035-5), DAPI (Sigma; #D9542) and the following primary antibodies against: WT1 (Abcam; #ab89901), CDH1 (BD Biosciences; #610181), RET (R&D Systems ; #AF1485), KRT19 (Abcam; #ab52625), CALB1 (Sigma; #C9848), PAX2 (Biolegend; #901001), GATA3 (Biocare Medical; #ACR405), PODXL (R&D Systems; #AF1658), and acetylated α-tubulin (Invitrogen; #720364). The secondary antibodies used were conjugated with Alexa 488, 568, 594, or 633 (Life Technologies). For staining of AVPR1A, sections were treated for antigen retrieval and incubated with an anti-AVPR1A antibody (Invitrogen; #720364) followed by an anti-rabbit secondary antibody conjugated with peroxidase polymers from an ImmPress Reagent Kit (Vector Laboratories; #MP-7401). The sections were then incubated with Alexa Fluor 594-tyramide (Thermo Fisher Scientific; #B40957) for 15 min at room temperature. Immunofluorescence was visualized using a TCS SP8 confocal microscope (Leica).

Analysis of cyst frequency in each segment of nephron organoids.

The numbers of glomeruli ($WT1^+$), proximal tubules ($LTL^+/CDH1^-$ or $LTL^+/CDH1^+$), and distal tubules ($LTL^-/CDH1^+$) were counted in immunostained cross-sections (three sections per organoid). Nephron segments in which the ratio of shortest lumen diameter to epithelial thickness was ≥1.5 were defined as cysts.

Measurement of UB stalk length

Using bright-field images of UB organoids at day 30, the lengths of the top four longest stalks in each organoid were averaged. Sixteen organoids per clone obtained from four independent experiments were analyzed.

Analysis of cyst frequency per stalk of UB organoids

The cyst percentages were measured against the total numbers of ureteric stalks emanating from the centers of individual UB organoids on bright-field images. Twelve organoids per clone obtained from three independent experiments were analyzed.

Quantitative RT-PCR analysis

RNA was isolated using an RNeasy Plus Micro Kit (Qiagen; #74034), and then reverse-transcribed with random primers and a Superscript VILO cDNA Synthesis Kit (Life Technologies; #11754050). Quantitative PCR was carried out using a Thermal Cycler Dice Real Time System (Takara Bio) and Thunderbird SYBR qPCR Mix (Toyobo; #QPS-201). Relative mRNA expression levels were analyzed by the ΔΔCT method and normalized to b-actin gene expression. The primers for qPCR are listed in Supplemental Table 1.

Supplemental Reference

1. Taguchi A, Nishinakamura R: Higher-Order Kidney Organogenesis from Pluripotent Stem Cells. *Cell Stem Cell* 21: 730-746.e6, 2017